Exhumation of the central Wasatch Mountains, Utah: 2. Thermokinematic model of exhumation, erosion, and thermochronometer interpretation

Todd A. Ehlers,[1,2] Sean D. Willett,[3] Phillip A. Armstrong,[4] and Davis S. Chapman[1]

Received 17 December 2001; revised 13 December 2002; accepted 13 December 2002; published 29 March 2003.

[1] The Wasatch fault is a ~370 km long normal fault in Utah that marks the boundary between the stable Colorado Plateau to the east and the extending Basin and Range to the west. Understanding the thermokinematic evolution of this fault can provide insights into intracontinental extensional tectonics and deformation processes in other rift zones (e.g., East Africa Rift, Transantarctic Mountains). We explore the thermokinematics of footwall exhumation and erosion in the Cottonwood Intrusive Belt of the central Wasatch Mountains. Emphasis is placed on using low-temperature thermochronometers to quantify (1) the spatial and temporal variability of exhumation and erosion rates, (2) the geometry of footwall tilt, (3) the fault dip angle, and (4) the magnitude and duration of exhumation. These processes are investigated using two-dimensional (2-D) thermal-kinematic models coupled with cooling-rate-dependent kinetic models which predict exhumed apatite fission track (AFT) and (U-Th)/He ages. The range of model parameters considered includes footwall exhumation and erosion rates at the fault between 0.2 and 2.0 mm yr^{-1}, footwall tilt hinge positions between 15 and 40 km distance from the fault, a single planar normal fault with dip angles of 45° and 60°, and exhumation magnitudes of up to 15 km at the fault. Simulations include the formation of a low thermal conductivity sedimentary basin and erosion of heat-producing layers. Erosion maintains a constant topographic profile. The kinematic and exhumation history of the Wasatch Mountains is investigated by comparing model predicted thermochronometer ages to observed AFT, ZFT, and (U-Th)/He ages. Predicted and observed ages are compared using a reduced chi-square analysis to determine a best fit kinematic model for the Wasatch Mountains. The preferred model includes exhumation occurring on either a 45° or 60° dipping fault, a footwall hinge located a minimum of 20–25 km from the fault, and a step decrease (deceleration) in the footwall exhumation rate at the fault from 1.2 to 0.8 mm yr^{-1} at around 5 Ma. The model also suggests an exhumation duration of ~12 Myr ± 2 Myr). *INDEX TERMS:* 1035 Geochemistry: Geochronology; 8010 Structural Geology: Fractures and faults; 8015 Structural Geology: Local crustal structure; 8109 Tectonophysics: Continental tectonics—extensional (0905); 8130 Tectonophysics: Heat generation and transport; *KEYWORDS:* exhumation, erosion, normal faults, numerical modeling, heat flow, thermochronometers

Citation: Ehlers, T. A., S. D. Willett, P. A. Armstrong, and D. S. Chapman, Exhumation of the central Wasatch Mountains, Utah: 2. Thermokinematic model of exhumation, erosion, and thermochronometer interpretation, *J. Geophys. Res.*, *108*(B3), 2173, doi:10.1029/2001JB001723, 2003.

1. Introduction

[2] Exhumation is an important geologic process responsible for the exposure of rocks and structures at the Earth's surface. In extensional tectonic regimes (e.g., Basin and Range province, East African Rift, or Transantarctic Mountains) most exhumation occurs in the footwalls of normal-fault bounded ranges. Several fundamental scientific questions apply to all tectonically active normal-fault bounded ranges, as follows: How fast is footwall exhumation? Are there spatial and temporal variations in the exhumation rate? How long has exhumation been active? We address these questions for the central Wasatch Mountains, Utah, but our modeling approach is applicable to other normal fault bounded ranges around the world. In this study we construct two-dimensional (2-D) thermokinematic numerical models of a normal-fault bounded range to explore the influence of spatially and temporally vari-

[1]Department of Geology and Geophysics, University of Utah, Salt Lake City, Utah, USA.
[2]Now at Department of Geological Sciences, University of Michigan, Ann Arbor, Michigan, USA.
[3]Department of Earth and Space Sciences, University of Washington, Seattle, Washington, USA.
[4]Department of Geological Sciences, California State University, Fullerton, Fullerton, California, USA.

0148-0227/03/2001JB001723$09.00

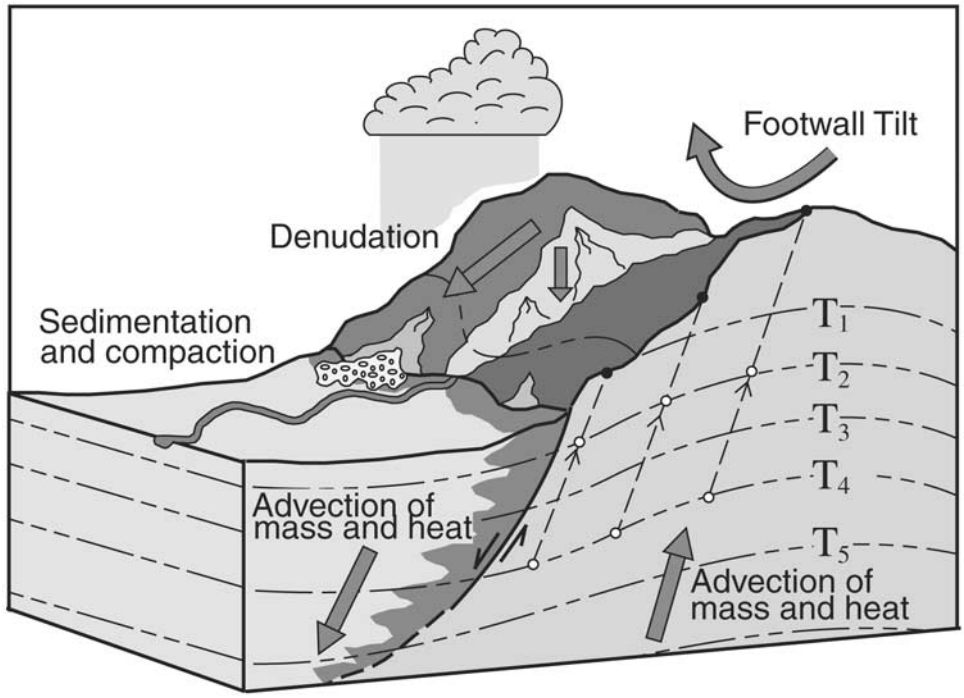

Figure 1. Thermal processes in normal fault bounded ranges that influence thermochronometric ages. Rocks in the subsurface (open circles) are exhumed and sampled at the surface (solid circles). Thermochronometer ages of sampled rocks depend on the depth to the closure temperature T_i and the exhumation rate. Isotherms (dashed lines) are deflected by the upward and downward advection of mass and heat in the footwall and hanging wall, respectively, and by relief on the nearly isothermal upper surface.

able exhumation rates, fault dip angles, and the duration of exhumation inferred from apatite and zircon fission track (AFT, ZFT) and apatite (U-Th)/He ages.

[3] The companion paper by *Armstrong et al.* [2003] presents the thermochronometer data used in this study, calculates thermal histories from track length modeling, and presents a structural synthesis for the Cenozoic evolution of the Cottonwood Intrusive Belt area of the Wasatch footwall block. *Armstrong et al.* [2003] interpret the spatial and elevation variations of thermochronometer ages to represent a two-stage tilt and exhumation history in which the locus of tilting and exhumation migrated westward. The first stage of tilt and exhumation occurred in Oligocene to middle Miocene time and primarily affected the middle and eastern parts of the range. The second stage began $\sim$10–12 Ma and affected the western 20 km of the range. In this paper, we address the thermokinematic evolution of only the second stage of tilt and exhumation.

[4] Other studies have investigated the thermokinematic effects of exhumation on thermochronometer cooling histories. *Stüwe et al.* [1994] and *Stüwe and Hintermüller* [2000] developed analytic expressions for the position of the AFT and apatite (U-Th)/He closure isotherms in the presence of eroding topography. *Mancktelow and Grasemann* [1997] investigated the effect of transient heat advection and topography on vertically exhumed thermochronometer samples. *Ehlers et al.* [2001] used a 2- D transient thermokinematic model of a normal-fault bounded range to compare differences in thermochronometer exhumation rates calculated from 2-D and conventional 1-D thermal models. Several studies have used 2-D thermal models of normal faults to document the effects of erosion and sedimentation rates on the thermal histories of hanging wall and footwall rocks [*Grasemann and Mancktelow*, 1993; *ter Voorde and Bertotti*, 1994; *Bertotti and ter Voorde*, 1994]. Two-dimensional thermal models, geobarometers and thermochronometers, were used by *van Wees et al.* [1992] to differentiate between pure, simple, and combined pure and simple shear modes of extension in the Beltic Zone, Spain.

[5] Previous studies have demonstrated that several fundamental thermal, kinematic, and surface processes influence the thermal history of exhumed thermochronometer samples (Figure 1). These processes include (1) upward and downward advection of mass and heat in the footwall and hanging wall, respectively, (2) heat refraction around low-conductivity sediments in the hanging wall basin, (3) lateral heat flow owing to topography, and (4) erosion of heat-producing layers. These processes all result in transient and 2-D heat flow and variable closure temperature depths across the footwall (e.g., T_2 and T_4, Figure 1) [*Ehlers et al.*, 2001].

2. Geologic Background

[6] The central Wasatch Mountains, the emphasis of this study, are located in the footwall of the Salt Lake City segment (Figure 2) of the Wasatch fault. The Wasatch fault has generated at least 10 surface-rupturing earthquakes ($6.8 < M < 7.3$) in the last 5600 years [*Swan et al.*, 1980; *McCalpin and Nishenko*, 1996; *Arabasz et al.*, 1992]. The geologic setting is described by *Armstrong et al.* [2003], and only the geologic features salient to the thermokinematic modeling are discussed here.

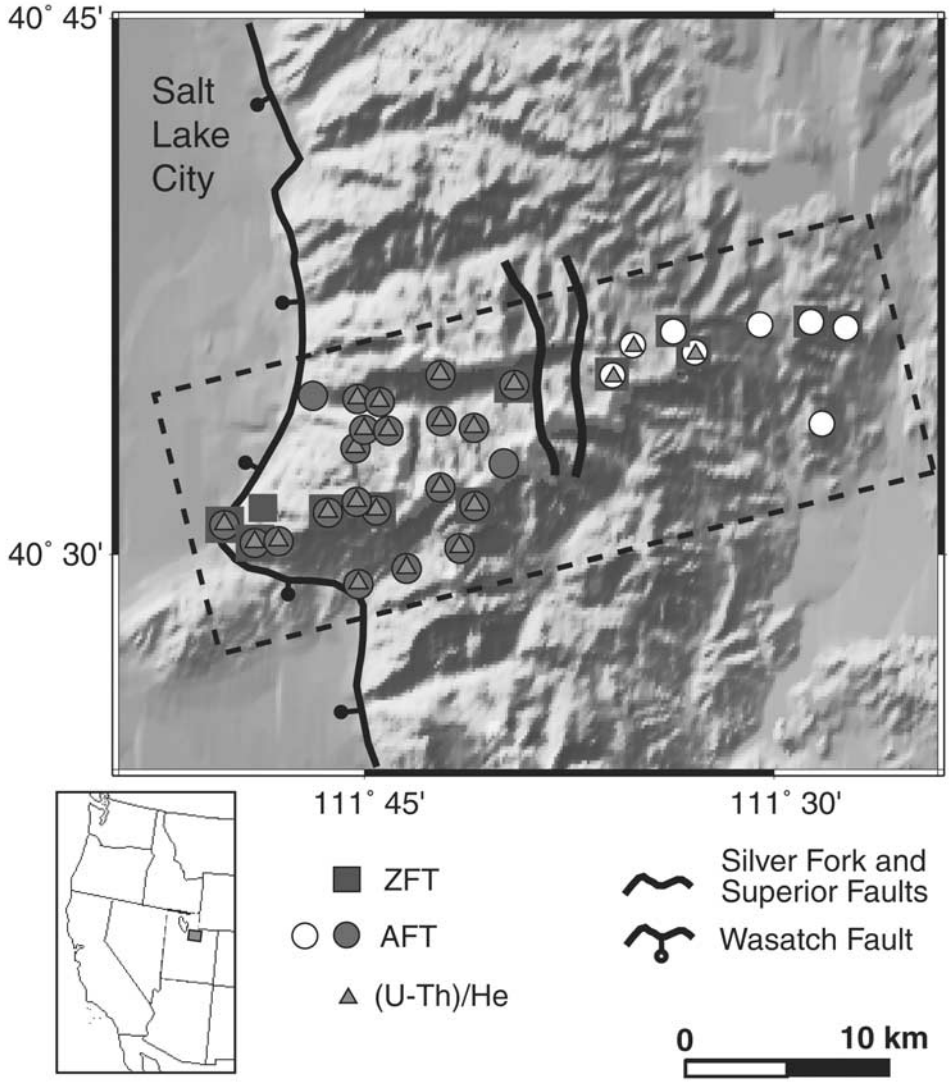

Figure 2. Central Wasatch Mountains with sample locations for zircon and apatite fission track, and (U-Th)/He ages considered in this study. Data are reported by *Armstrong et al.* [2003]. Multiple thermochronometer analyses were conducted on the same rock samples for most locations.

[7] Oligocene age granitoid plutons were intruded into older sedimentary strata and are the source of all but one sample dated of *Armstrong et al.* [2003]. The one other sample came from the Proterozoic Little Willow Formation. Unconsolidated sediments on the hanging wall are estimated to be ~1.5 km thick based on inversion of gravity data assuming a simple two layer density structure [*Zoback*, 1983; *Radkins*, 1990]. The thickness of consolidated hanging wall sedimentary rocks is not well determined. Topographic relief between the valley floor and range crest is ~2 km. Topographic relief between transverse canyons and ridges is ~1.0–1.5 km.

[8] Numerous studies address, with conflicting results, the magnitude and rate of exhumation of the central Wasatch Mountains (Table 1). *Parry and Bruhn* [1987] summarized previous estimates of the exhumation which range from 1.5 km based on topographic relief [*Eardley*, 1939] to 12 km based on eroded stratigraphic section [*King*, 1878]. Some of these studies are discrepant because they

Table 1. Previous Estimates of Exhumation Magnitude and Rate

Exhumation Magnitude, km	Method	Study
12	stratigraphic	*King* [1878]
>11	geochemical	*Parry and Bruhn* [1987]
3.0–4.6	stratigraphic	*Crittenden* [1964]
3.0–4.0	topography, basin fill	*Gilbert* [1928], *Hintze* [1971], and *Zoback* [1983]
1.5–3.0	geomorphic	*Davis* [1903], *Marsell* [1932], and *Eardley* [1933, 1939
Vertical Exhumation Rate, mm/yr	**Method**	**Study**
0.7–0.8[a]	fault-trenching	*Schwartz and Coppersmith* [1984]
0.3–0.5[a]	paleoseismology	*Machette et al.* [1991]
0.7	K-Ar, fluid inclusions	*Parry and Bruhn* [1987]
0.2–0.8	apatite fission track	*Evans et al.* [1985] and *Kowallis et al.* [1990]
~0.05[a]	shallow seismic	*Crone and Harding* [1987]

[a]Assumes the exhumation rate is one-half the net tectonic vertical displacement.

report surface uplift rather than exhumation. Uncertainty also exists in estimates of the exhumation rate. Rates of footwall vertical exhumation span several orders of magnitude and range between 0.05 mm yr^{-1} based on shallow seismic imaging of offset Holocene strata [*Crone and Harding*, 1987] and 0.8 mm yr^{-1} from K-Ar and AFT thermochronometry [*Evans et al.*, 1985; *Kowallis et al.*, 1990]. Some of the discrepancy in previous exhumation rate estimates (Table 1) may result from differences in the timescale the methods are sensitive to. For example, paleoseismology studies using offset markers in fault trenches or shallow seismic studies deduce rates over the timescale of individual earthquake ruptures (10^3 years), whereas thermochronometer studies are sensitive to processes on significantly longer timescales (10^6–10^7 years). A primary objective of this study is to refine estimates of exhumation rates on million year timescales by integrating new thermochronometer data with a thermokinematic model of footwall exhumation.

3. Thermochronometer Data

[9] Zircon and apatite fission track and apatite (U-Th)/He ages have closure temperatures of ~240°C, 120°C, and 70°C, respectively, thus providing constraints on exhumation histories over this temperature range [*Naeser*, 1979; *Naeser et al.*, 1989; *Parrish*, 1983; *Yamada et al.*, 1995; *Farley*, 2000; *Gleadow and Brown*, 2000]. Kinetic models for thermal annealing of apatite fission tracks are well developed [*Naser and Faul*, 1969; *Wagner and Reimer*, 1972; *Laslett et al.*, 1987; *Green et al.*, 1986; *Carlson*, 1990; *Crowley et al.*, 1991], with variations in annealing behavior arising from compositional variations and crystallographic anisotropy [*Green et al.*, 1985; *Donelick et al.*, 1999; *Carlson et al.*, 1999; *Ketcham et al.*, 1999]. Helium produced in apatite by the spontaneous decay of ^{238}U, ^{235}U, and ^{232}Th is lost by volume diffusion, thus serving as the basis for (U-Th)/He dating [*Zeitler et al.*, 1987; *Farley et al.*, 1996; *Wolf et al.*, 1996, 1998; *Farley*, 2000]. Below temperatures of ~300°C, the diffusivity of apatite is described by a linear, temperature-dependent Arrhenius relationship.

[10] *Armstrong et al.* [2003] report new AFT, ZFT, and (U-Th)/He data which provide the most complete picture of exhumation to date for the Wasatch Mountains. We use 30 AFT, 7 ZFT, and 22 (U-Th)/He ages from *Armstrong et al.* [2003] (dashed box, Figure 2). Five additional ZFT data located close to the fault from *Kowallis et al.* [1990] were used to augment new ZFT data collected from greater distances from the fault. The data from *Armstrong et al.* [2003] suggest a northward tilt of several degrees which precludes inclusion of samples from north of the dashed box in our 2-D model.

[11] The thermochronometer data are shown in Figure 3 with sample age plotted versus distance from fault along an azimuth of 070°. This azimuth is perpendicular to the general trend of the range front and fault (Figure 2) and in the direction of fault slip. The ZFT data range from 10 Ma at the fault to 37 Ma at 24 km away from the fault (Figure 3a). At distances >10–15 km from the fault, the ZFT ages are concordant with intrusion U-Pb ages [*John*, 1989; *Constenius*, 1998]. Unlike the AFT and apatite (U-Th)/He thermochronometer systems the ZFT system does not have an established kinetic model for track annealing. This study will primarily focus on the AFT and (U-Th)/He systems for which kinetic models are established and can be coupled with thermokinematic models to compare predicted ages to observed ages. Despite uncertainties in the kinetics of ZFT annealing, the ZFT data are of use for delineating the duration of faulting on the Wasatch fault (see section 6.2).

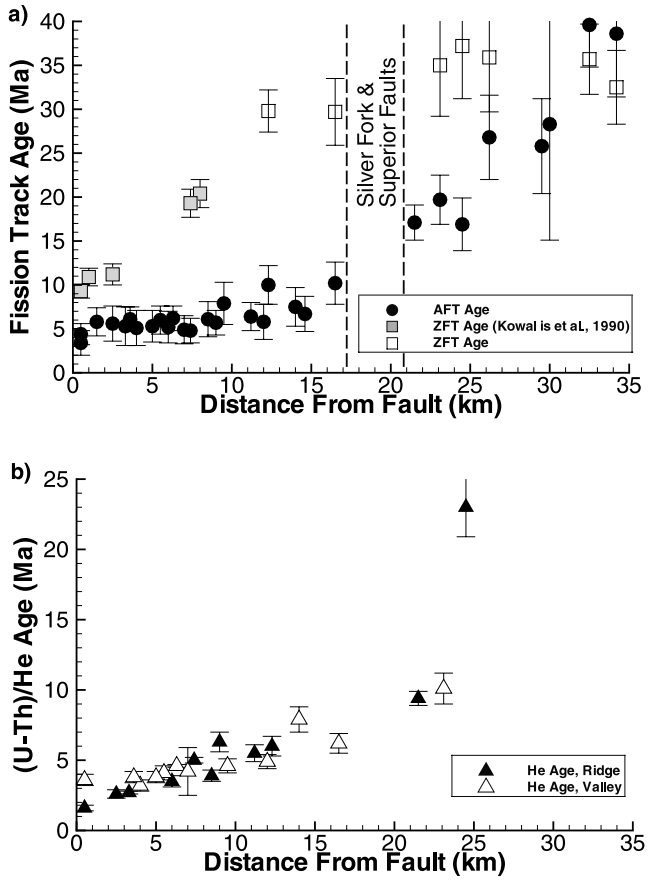

Figure 3. Thermochronometer age versus distance east of Wasatch fault along a bearing of 070° (Figure 2). (a) ZFT and AFT ages with 2 SD uncertainties in sample ages. (b) (U-Th)/He ages. Error bars represent uncertainties in sample ages based upon analytic uncertainties and replicate analysis [*Armstrong et al.*, 2003].

[12] The AFT ages range from 3.4 Ma adjacent to the fault to 39.6 Ma at 32 km away from the fault (Figure 3a). Long (13.7–15.3 μm) fission tracks and track length modeling [*Armstrong et al.*, 2003] suggest that the samples located at distances between 20 and 27 km from the fault (open circles) were exhumed rapidly during an earlier (late Oligocene to middle Miocene) cooling event associated with several kilometers of exhumation east of the Silver Fork and Superior faults. Samples located at >27 km from the fault were initially intruded above the partial annealing zone (PAZ) [*Armstrong et al.*, 2003] and record the age of crystalization. AFT ages at distances >20 km record a cooling event that occurred earlier than the exhumation of the western 20 km of the Wasatch Mountains. Therefore only the AFT data within 20 km of the fault are used in this study constrain the thermokinematic models.

[13] (U-Th)/He ages are ~1.6 Ma adjacent to the Wasatch fault and increase nearly monotonically to 10.1 Ma at 23 km distance from the fault (Figure 3b). The increase of (U-Th)/He, AFT, and ZFT ages with distance from the fault is interpreted to result from footwall tilt such that samples adjacent to the fault were exhumed from greater depths and faster than samples at greater distances from the fault. The (U-Th)/He ages of samples collected at similar distances from the fault at ridge versus valley elevations (Figure 3b) typically differ by ~1 Myr. This variation may be due to elevation differences at a common distance from the Wasatch fault. These elevation-age relationships are investigated for a north-south elevation transect between Little Cottonwood Canyon and Lone Peak (Figure 5b of *Armstrong et al.* [2003]). The slope of a best fit line in this age-elevation plot is 1.2 mm yr^{-1}. This change in age with elevation was used to correct (U-Th)/He ages to a common sample elevation [*Armstrong et al.*, 2003, Figure 5c]. The elevation correction changes (U-Th)/He ages by <1 Myr, an amount typically within the uncertainties of ages. After this correction the (U-Th)/He ages still vary as a function of horizontal distance from the fault, with elevation-related changes being small at any distance from the fault. This small north-south topographic relief effect on (U-Th)/He ages is probably related to the isotherms sensing the topography which in turn leads to relatively high elevation-age gradients locally (see section 6.1)[also see *Ehlers et al.*, 2001; *Braun*, 2002]. However, in this study we emphasize the longer wavelength variations in sample ages related to movement of the Wasatch fault. Future work will investigate shorter wavelength variations in sample ages related to canyon and ridge topography.

4. The Model

[14] The simplest assumption for thermochronometer interpretation is that samples are exhumed vertically toward a horizontal surface through a 1-D steady state thermal field. A more realistic assumption in tectonically active regions is that exhumation trajectories have both vertical and horizontal components and that the thermal field is transient and multidimensional [e.g., *Ehlers et al.*, 2001; *Batt et al.*, 2001; *Batt and Brandon*, 2001]. The 2-D nature of the thermal field surrounding the Wasatch normal fault is discussed in detail by *Ehlers and Chapman* [1999] and *Ehlers et al.* [2001]. There are three components to our model: (1) a thermal model that predicts temperatures as a function of space, time, and the kinematic velocity field, (2) a kinematic model describing particle motions, and (3) a thermochronometer kinetic model that calculates predicted ages of exhumed rocks. The thermal, kinematic, and kinetic models used in this paper are described in detail in sections 4.1–4.3.

4.1. Thermal Model

[15] The background thermal field of the crust is controlled primarily by heat flow into the base of the crust and thermophysical properties of the crust (conductivity, heat production, heat capacity). For the central Wasatch Mountains we assume that 2-D transient heat transfer occurs by conduction and advection of rock in response to footwall erosion and hanging wall sedimentation. These thermal processes are described by the advection-diffusion equation:

$$\frac{\nabla(K\nabla T)}{\rho c} - \bar{v}\nabla T - \frac{\partial T}{\partial t} = -\frac{A}{\rho c}, \qquad (1)$$

where $\bar{v}$ is the material velocity, T is temperature, and t is time. K, ρ, c, and A are the thermal conductivity, density, specific heat, and radiogenic heat production per unit volume, respectively.

[16] Equation (1) is solved in an Eulerian (spatial) reference frame using the finite difference scheme described by *Ehlers and Chapman* [1999]. A representative topographic profile perpendicular to the range front (Figure 2) is used for the top boundary of the model. The topographic profile remains constant throughout simulations by assuming a topographic steady state such that the erosion rate is equal in magnitude to the tectonic rock uplift rate. Our steady state topography assumption is supported by landform evolution modeling studies of normal fault bounded ranges in the Basin and Range that suggest topographic steady state is reached within ~2 Myr of the onset of faulting [*Densmore et al.*, 1998; *Allen and Densmore*, 2000]. We demonstrate later (section 6.2) that the Wasatch fault has been active for significantly longer (12 ± 2 Myr) than this 2 Myr period of inferred transient topography. Therefore the effects of transient topography on AFT and (U-Th)/He cooling ages most likely ended long before closure of AFT and (U-Th)/He samples from the Wasatch (Figure 3), and the assumption of steady state topography should not influence our interpretation of the data.

[17] Pleistocene glaciation of the Wasatch Mountains is the only other erosional process that may have significantly modified the topography and affected cooling ages. However, glaciation will most likely not influence our interpretation of (U-Th)/He cooling ages because (1) the magnitude of glacial over deepening in Little Cottonwood Canyon, where the samples came from, does not appear to be significant compared to neighboring canyons which are unglaciated and have similar relief between canyons and ridges (e.g., Mill Creek Canyon), and (2) if for unforeseen reasons glaciation did influence cooling ages, our implementation of an average topographic profile (Figure 5) across the Wasatch will minimize the effect of changes in local relief induced by glaciation.

[18] Changes in material properties in the thermal model are accounted for by tracking material points in a Lagrangain (material) reference frame. This formulation allows for erosion of heat producing material and formation of a low-thermal conductivity sedimentary basin. Thus the contribution of heat production to surface heat flow decreases with time as the exhumation duration increases. Model parameters and material properties used in this study are summarized in Table 2. We assume heat production roughly obeys an exponential decrease with depth which is consistent with Basin and Range heat production models [*Lachenbruch and Sass*, 1977]. Our assumed heat production profile was validated with 20 representative samples analyzed from the central Wasatch Mountains (Appendix A). Published thermal conductivity measurements near the Wasatch Mountains suggest an average value of 3.3 ~± 1.0) W m^{-1} K^{-1} at 25°C [*Deming*, 1988; *Bodell*, 1981; *Moran*, 1991; *Powell*, 1997]

Table 2. Numerical Model Parameters

	Model Input Value
Material Properties	
Country rock thermal conductivity	3.0 W m^{-1} k^{-1}
Basin Thermal Conductivity	2.2 W m^{-1} K^{-1}
Density	3000 kg m^{-3}
Specific Heat	1000 J kg^{-1} K^{-1}
Heat production z	
Sedimentary rocks (0–6 km)	1.0 μW m^{-3}
Upper crust (6–16 km)	$A = A_0 \exp(-z/R)$
	A_0 = 2.5 μW m^{-3}, R = 10 km
Lower crust (16–26 km)	0.6 μW m^{-3}
Mantle (26–40 km)	0.1 μW m^{-3}
Numerical Parameters	
Time step size	100 years
Horizontal node spacing	130 m, 150[a] m
Vertical node spacing	225 m, 150[a] m
Valley surface temperature	15°C
Range surface temperature	15–7°C/km × height (km)
Basal heat flow	0.06 W m^{-2}
Initial surface heat flow	0.09 W m^{-2}
Model domain width, depth	120 km, 40 km

[a]Used in 45°Fault simulations.

(see also Appendix A). We assume in our model a slightly lower representative crustal thermal conductivity of 3.0 W m^{-1} K^{-1} because thermal conductivity decreases 0.1–0.5 W m^{-1} K^{-1} with increased temperature and depth in the crust [*Buntebarth*, 1991; *Clauser and Huenges*, 1995]. A thermal conductivity of 2.2 W m^{-1} K^{-1} is assumed for the sedimentary basin.

[19] The boundary conditions in the model include a constant basal heat flux of 60 mW m^{-2} and no-flux boundary conditions on the sides (Figure 4a). The upper boundary has a constant surface temperature in the valley and an elevation-dependent temperature in the range. The sum of our assumed basal and radiogenic heat flow provide an initial surface heat flow of 90 mW m^{-2}. This surface heat flow is consistent with present-day measurements near the Wasatch Mountains [*Sass et al.*, 1994; *Ehlers and Chapman*, 1999] and paleothermal gradient estimates from exhumed fluid inclusions in the central Wasatch Mountains [*Parry and Bruhn*, 1987]. Initial temperatures are specified as the conductive steady state solution for the specified boundary conditions.

4.2. Kinematic Model

[20] The kinematics of a normal-fault bounded range include horizontal extension and footwall and hanging wall tilt. We define the 2-D kinematic model in the reference frame of the fault. A horizontal velocity component, V_x, is prescribed as constant and opposite in magnitude across the fault (x = 0), thereby providing symmetric displacement around the fault (Figure 4b). In the footwall the horizontal component is prescribed as:

$$V_x = V_{\text{Extension}}, \tag{2}$$

where $V_{\text{Extension}}$ is one half the horizontal displacement rate across the fault. The extension rate, $V_{\text{Extension}}$, and fault dip angle define exhumation rates in the footwall. Because the exhumation rate is a fundamental control on the cooling rate of exhumed thermochronometer samples we characterize the exhumation rate of the footwall using the maximum exhumation rate, $V_{z\text{max}}$, which is given by

$$V_{z\text{max}} = V_{\text{Extension}} \tan\beta, \tag{3}$$

where β is the fault dip angle. Footwall tilt is described using a vertical velocity component, V_z, that is largest in magnitude adjacent to the fault ($V_{z\text{max}}$) and decays linearly with distance x from the fault (Figure 4b) such that

$$V_z = V_{z\text{max}}\left(1 - \frac{1}{X_{\text{Hinge}}}x\right), \quad (0 \le x \le X_{\text{Hinge}}), \tag{4}$$

where X_{Hinge} is the footwall hinge distance from the fault where V_z = 0. This kinematic field is prescribed as a function of distance from the fault at all depths in the thermal model such that the footwall hinge parallels the fault (Figure 4a). In the following sections we describe predicted thermochronometer ages in terms of the exhuma-

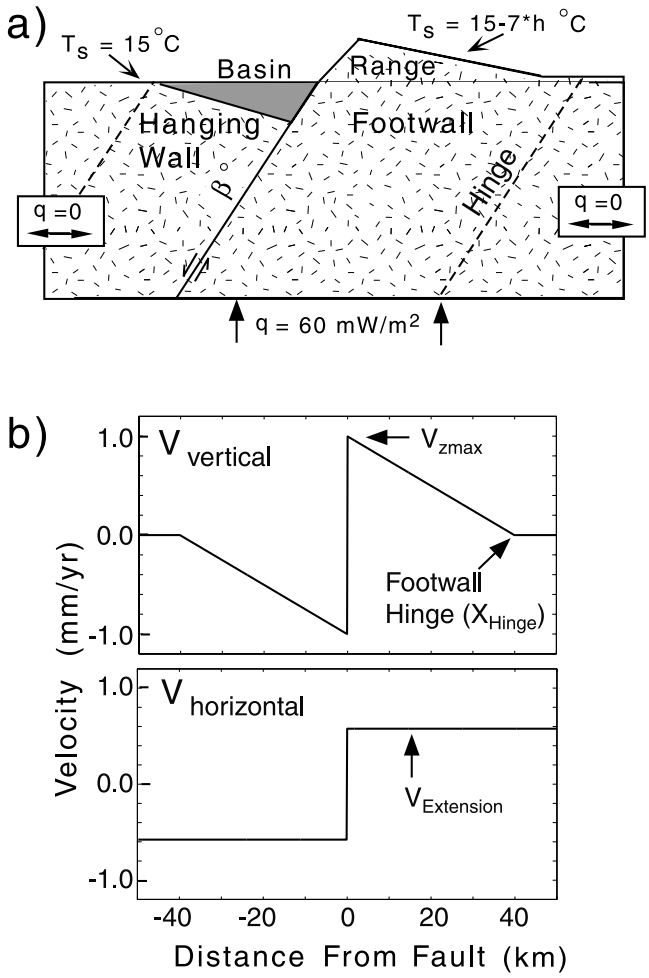

Figure 4. Model geometry used for 2-D thermokinematic modeling. (a) Thermal model geometry and prescribed boundary conditions. The q denotes a flux boundary condition and T_s is the surface temperature boundary condition. (b) Functional form of the assumed vertical and horizontal components of the velocity field used to drive advective heat transfer.

tion rate at the fault, $V_{z\max}$. However, note that exhumation rates vary across the footwall (equation (4)).

[21] Three parameters define our footwall kinematic field (Figure 4b and equations (2), (3), and (4)): (1) the footwall exhumation rate at the fault ($V_{z\max}$); (2) the distance of the footwall hinge from the fault (X_{Hinge}); and (3) the fault dip angle, β. We investigated footwall exhumation rates at the fault of 0.2–2.0 mm yr^{-1}, footwall hinge positions between 15 km and 40 km from the fault, and fault dip angles of 45° and 60°. This description of the kinematic field focuses on the footwall where we have thermochronometer samples. We also prescribe the hanging wall kinematic field in a similar manner (Figure 4b) for the thermal model calculation.

[22] Our assumed kinematic model imposes extensional strain on the hanging wall and footwall. The effect of this strain on rock exhumation pathways is discussed in section 5.1. The assumed kinematic model and associated strain is justified by field observations from the Wasatch Mountains (Big Cottonwood Formation) where numerous small faults and joints with ~1–10 m normal sense offset are located between the fault and 10+ km distance from the fault in the footwall (unpublished results from *Ehlers and Chan* [1999]). Furthermore, extensional strain has been observed in the hanging wall of the Wasatch Fault. For example, the West Valley Fault is an active antithetic fault in the Salt Lake Valley and accommodates extension of the hanging wall [*Hecker*, 1993; *Keaton et al.*, 1993]. Thus the extensional deformation imposed by our kinematic model on the hanging wall and footwall is consistent with observed distributed strain in the central Wasatch Mountains and Salt Lake Valley. As discussed below, the assumed kinematic model has the additional advantage of easily tracking exhumation trajectories in two dimensions.

[23] Equations (2) and (4) are simple enough to derive analytic expressions for particle positions in the footwall during the exhumation process. Particle positions can be tracked forward in time from an initial position (X_0, Z_0) to a new position (X_1, Z_1) after a specified time (Δt):

$$X_1 = V_x \Delta t + X_0 \tag{5}$$

$$Z_1 = Z_o - \int_{t_o}^{t_1} (V_z x) dt. \tag{6}$$

V_z retains the integral form because V_z is a function of x. Because V_x is constant, this can be written as

$$Z_1 = Z_o - \int_{x_o}^{x_1} \frac{V_z}{V_x} dx, \tag{7}$$

which can be solved analytically by substitution of equations (2) and (4). Equations (5) and (7) are used to incrementally track the position and temperature of particles at each time step as they are exhumed toward the surface. The temperature history of particles exhumed to the surface is then used to predict (U-Th)/He and AFT ages using thermochronometer kinetic models.

4.3. Thermochronometer Kinetic Models

[24] Apatite fission track and (U-Th)/He ages can be predicted from thermal histories using kinetic models for track annealing and helium diffusion, respectively. Kinetic models of apatite fission track annealing have been documented in numerous studies [*Naser and Faul*, 1969; *Wagner and Reimer*, 1972; *Laslett et al.*, 1987; *Green et al.*, 1986; *Carlson*, 1990; *Crowley et al.*, 1991; *Ketcham et al.*, 1999]. The apatite samples considered in this study are fluorapatite [*Armstrong et al.*, 2003] so we assume a fluorapatite annealing model based on the data of *Green et al.* [1986], fit by *Laslett et al.* [1987], and implemented by *Willett* [1992, 1997].

[25] Recent advances have been made in quantifying the kinetics of helium diffusion in apatite [*Zeitler et al.*, 1987; *Farley et al.*, 1996; *Wolf et al.*, 1996, 1998; *Farley*, 2000]. We use these kinetic parameters to calculate predicted (U-Th)/He ages assuming diffusion of helium in a spherical grain. Spherical diffusion can be described by [*Carslaw and Jaeger*, 1959; *Wolf et al.*, 1996, 1998]

$$\frac{\partial H}{\partial t} - \frac{D}{a^2}\left[\frac{\partial^2 H}{\partial r^2} + \frac{2}{r}\cdot\frac{\partial H}{\partial r}\right] = 8\lambda_{238}{}^{238}U + 7\lambda_{235}{}^{235}U + 6\lambda_{232}{}^{232}Th, \tag{8}$$

where H represents the ^4He concentration in a domain with radius a as a function of time (t), and radial position (r) normalized by the diffusion domain size. The three right hand terms in equation (8) account for ^{4}He produced by radiogenic decay of ^{238}U, ^{235}U, and ^{232}Th with associated decay rate constants λ. The temperature-dependent diffusivity, D, is calculated as

$$D = D_0 \exp[-E_a/RT(t)], \tag{9}$$

where D_0 and E_a are the empirically derived diffusivity at infinite temperature and activation energy, respectively [*Farley*, 2000], R is the gas constant, and $T(t)$ is temperature.

[26] Equations (8) and (9) were solved numerically using a spherical finite element model to generate predicted (U-Th)/He ages. The model was validated using analytic solutions for isothermal ingrowth diffusion [*Carslaw and Jaeger*, 1959; *Ozisik*, 1989] and compared to the California Institute of Technology helium diffusion algorithm (K. Farley and M. House, personal communication, 2000). We assumed Durango fluorapatite kinetic parameters of E_a = 33 kcal mol^{-1}, and $D_0 = 50 \times 10^8$ μm^2 s^{-1} [*Farley*, 2000]. The average grain diameter of the Wasatch samples is 85 μm [*Armstrong et al.*, 2003] which we assume to be representative of all samples. Initial ^{238}U and ^{232}Th concentrations of 20 ppm were used. Thermochronometer samples were given an initial intrusion age of 35.5 Ma based on the average pluton ages of the Little Cottonwood and Alta Stocks.

5. Results

5.1. Two-Dimensional Thermokinematic Field and Predicted Ages

[27] As parametrized in our model the particle paths, thermal histories, and thermochronometer ages of specific material points depend on the exhumation rate of the footwall at the fault ($V_{z\max}$), the footwall hinge position, the fault dip angle and the total duration of fault motion. Figure 5 shows particle paths and temperature histories with a 45° fault dip, with a footwall exhumation rate at the

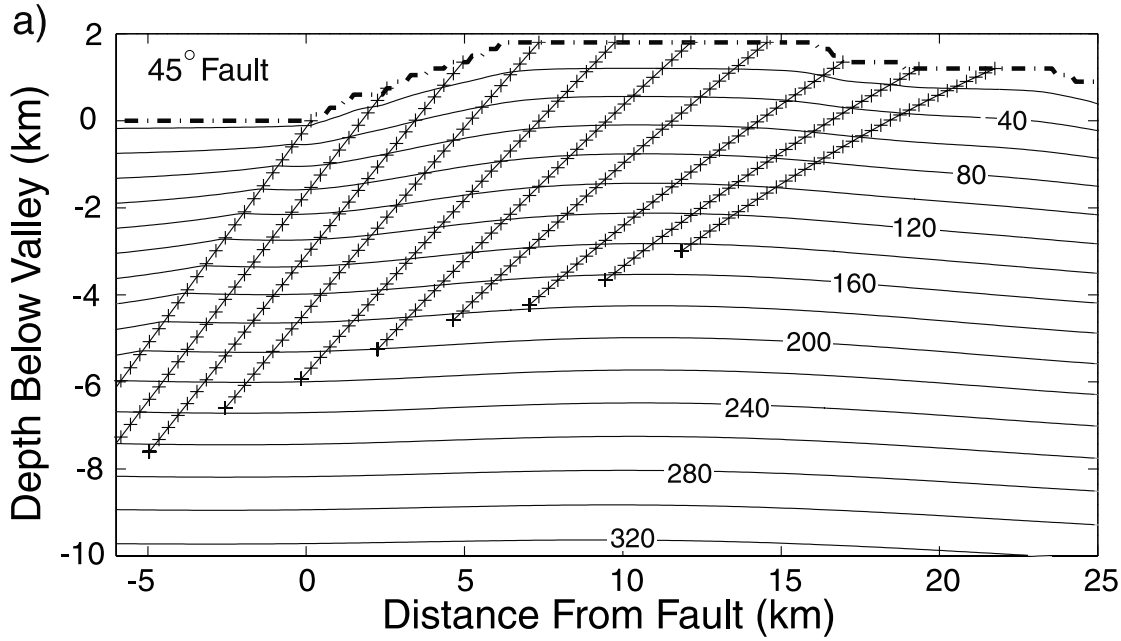

Figure 5. Example output from the coupled thermokinematic model for a 45° dipping fault. Bold dashed line representing the surface is the average topographic profile of the central Wasatch Mountains. Isotherms (solid lines) show subsurface temperatures (°C) after 16.5 Myr of fault motion with a maximum vertical velocity, V_{zmax}, of 0.6 mm yr^{-1} and a footwall hinge located at 30 km. Pluses represent progressive position of particles in 0.5 Myr increments.

fault of 0.6 mm yr^{-1} μm^{-1}, a footwall hinge located 30 km from the fault, and a total faulting duration of 16.5 Myr The position of exhumed particles at 0.5 Myr increments (crosses) is shown with the resultant temperature field. The deepest rocks are exhumed adjacent to the fault and there is progressively less total exhumation away from the fault.

[28] Isotherms are curved and 2-D heat flow occurs (Figure 5). For example, at a distance of 5 km from the fault and near the (U-Th)/He closure temperature of 60°C (−0.4 km) the vertical and horizontal components of heat flow are ~88 and 15 mW m^{-2}, respectively. Lateral heat flow is ~17% that of the vertical heat flow and is therefore significant. Lateral heat flow becomes even more significant at higher exhumation rates because isotherms are swept closer to the topography [e.g., see *Ehlers et al.*, 2001, Figure 5]). Thermochronometer sample cooling rates in the model also decrease away from the fault from 24°C Myr^{-1} at the fault to under 10°C Myr^{-1} 25 km into the footwall.

[29] The distance a particle travels laterally before reaching the surface depends on the extension rate and fault dip angle. For example, with a 45° dipping fault a particle exhumed to the surface at a distance of 20 km from the fault travels 10 km laterally during exhumation. For a 60° fault, a particle exhumed to the surface at the same distance from the fault has travelled 5 km laterally. For the topography and isotherms shown in Figure 5, lateral motion results in particle motion oblique to the isotherms. Thermochronometer ages are calculated by integrating the sample's temperature history. Therefore lateral motion results in older ages than if they were exhumed on vertical trajectories because samples spend more time in the PAZ.

[30] An example of predicted AFT ages is shown in Figure 6a (solid lines) for a 45° dipping fault with a footwall hinge located at a distance of 25 km from the fault, 10 km of vertical exhumation at the fault, and a range of footwall exhumation rates at the fault (V_{zmax}). The individual effects of the other parameters on exhumed rock ages are discussed in the following sections. The AFT data from the Wasatch are shown for comparison. The youngest predicted AFT ages of rocks occur adjacent to the fault and the ages increase slowly with distance from the fault out to ~20 km distance. Between 20 and 25 km from the fault, the predicted AFT ages increase rapidly. At distances greater than ~25–35 km from the fault, the ages have a constant value of ~35 Ma. Samples located at distances <20 km from the fault are interpreted as being fully annealed prior to exhumation. The predicted ages between 20 and 25 km distance from the fault indicate particles exhumed from the PAZ. Particles exhumed at distances >25 km from the fault record intrusion ages and experienced only a small amount of exhumation.

[31] Variations in predicted ages at different distances from the fault strongly depend on the exhumation rate of the footwall at the fault (V_{zmax}), the footwall hinge distance, total duration of fault motion and, to a lesser extent, on the fault dip angle. The effect of each of these parameters is discussed below.

5.2. Effect of Footwall Exhumation Rate on Ages

[32] Figure 6 demonstrates the effect of the footwall exhumation rate, as indicated by V_{zmax}, on ages of exhumed samples. Predicted exhumed AFT and (U-Th)/He sample ages are shown for V_{zmax} between 0.2 and 2.0 mm yr^{-1} with a 10 km magnitude of exhumation adjacent to the fault. Fixing the magnitude of exhumation implies a variable duration of faulting for each set of predicted ages in

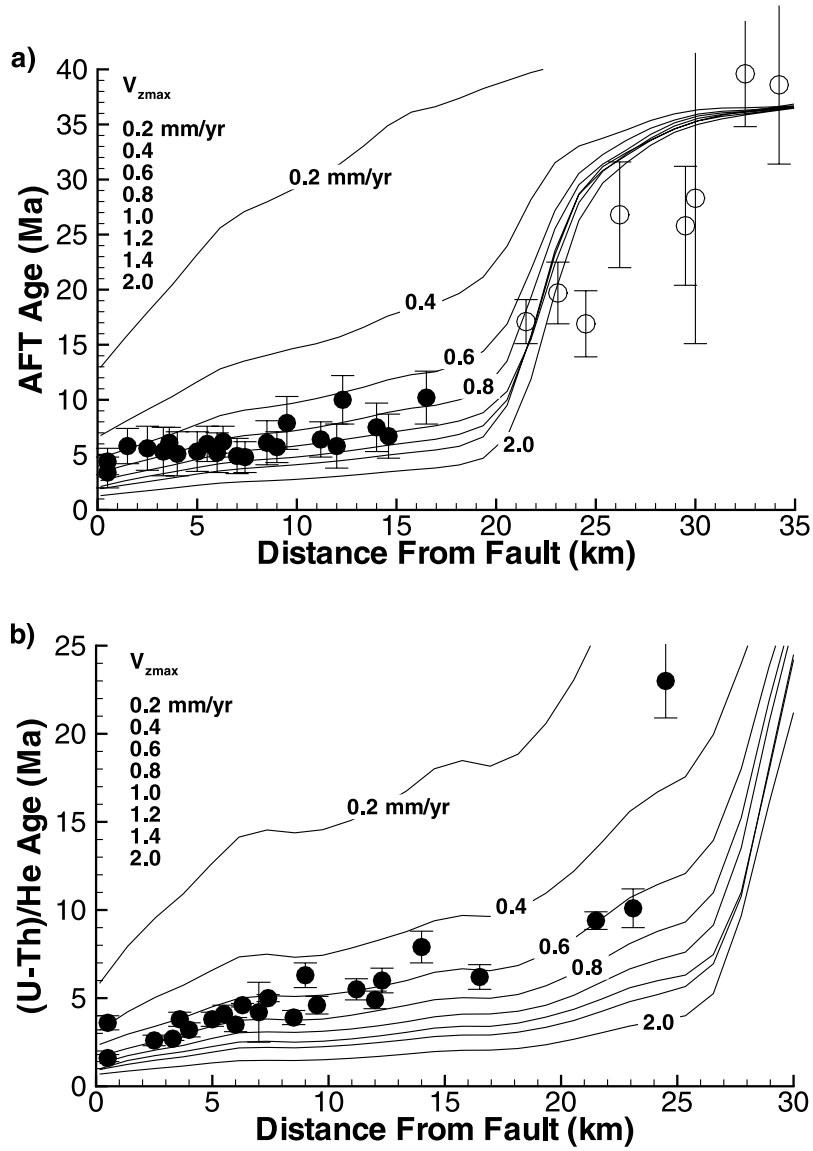

Figure 6. Effect of changing exhumation rate on model predicted thermochronometer ages. Fixed parameters include the hinge position at 25 km and a 45° dipping fault. (a) Predicted and observed AFT ages versus distance from fault. (b) Predicted and observed (U-Th)/He ages versus distance from fault. Solid lines represent predicted thermochronometer ages for footwall exhumation rates at the fault (V_{zmax}, equation (3)) between 0.2 and 2.0 mm yr^{-1}. All predicted thermochronometer ages were assumed to have initial intrusion ages of 35.5 Ma. Open circles in Figure 6a represent samples that cooled during an earlier event (see text).

Figure 6. For example, the 0.8 and the 1.2 mm yr^{-1} curves have faulting durations of 12.5 and 8.3 Myr, respectively.

[33] Increasing the footwall exhumation rate at the fault (V_{zmax}) results in a younger age at any point on the footwall (Figure 6a). For example, when V_{zmax} is 0.4 mm yr^{-1}, AFT ages vary from 6.5 to 17 Ma at distances of 0–15 km from the fault. When V_{zmax} is 2.0 mm yr^{-1}, (U-Th)/He ages range from 1 to 3 Ma over the same distance. Ages decrease with increased exhumation rates because cooling of the footwall due to advection is much faster relative to conduction and, therefore, rocks do not cool through closure temperatures until they are very near the surface.

[34] The predicted (U-Th)/He ages show a similar gradual increase in predicted age with increased distance from the fault (Figure 6b). One notable difference between the predicted AFT and (U-Th)/He ages is the greater variance in predicted (U-Th)/He ages due to topographic effects. For example, peaks and troughs in the 0.6 mm yr^{-1} (U-Th)/He curve (Figure 6b) are a result of topographic variations (Figure 5) in the direction of the transect. The irregularity in the predicted age curve decreases with increased exhumation rates because isotherms are advected farther upward, resulting in a higher and more constant thermal gradient and almost homogeneous ages.

[35] Comparison of predicted and observed (U-Th)/He ages suggests a footwall exhumation rate at the fault, V_{zmax}, of ~0.6 mm yr^{-1}. In comparison, the AFT data (Figure 6a) suggest a higher V_{zmax} of ~0.8 mm yr^{-1}. These differences

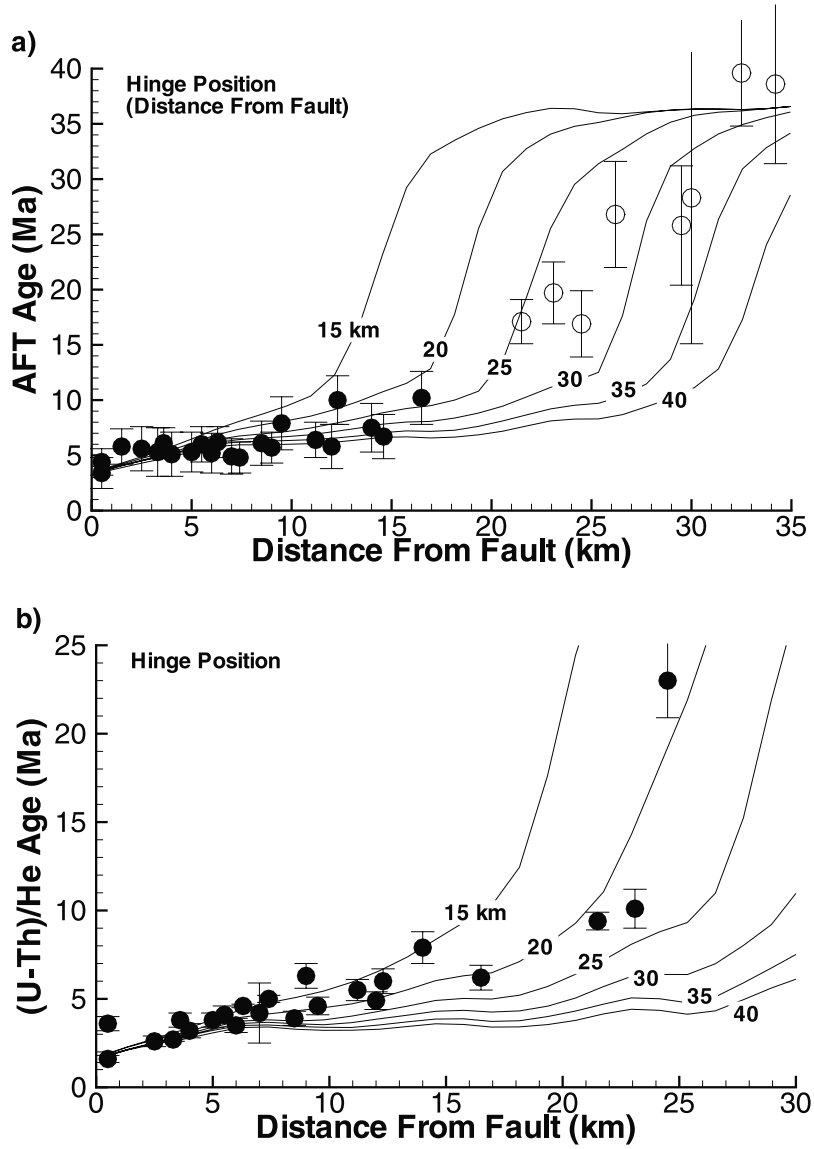

Figure 7. Effect of footwall hinge position on predicted thermochronometer ages. Fixed parameters include a footwall exhumation rate at the fault (V_{zmax}, equation (3)) of 0.8 mm yr^{-1} and a 45° dipping fault. (a) Predicted (solid lines) and observed AFT ages versus distance from fault. (b) Predicted (solid lines) and observed (U-Th)/He ages. Hinge positions from 15 to 40 km are shown. All samples were assumed to have initial intrusion ages of 35.5 Ma Open circles in Figure 7a represent samples that cooled during an earlier exhumation event (see text).

in V_{zmax} could be interpreted to suggest a 0.2 mm yr^{-1} deceleration in the exhumation rate from ~5 Ma to present. We quantitatively explore this inference in more detail later.

5.3. Effect of Footwall Hinge Position on Ages

[36] Figure 7 shows the effect of the footwall hinge position on thermochronometer ages for models with a 45° dipping fault and a footwall exhumation rate at the fault (V_{zmax}) of 0.8 mm yr^{-1}. Results are shown following 10 km of exhumation at the fault. Increasing the hinge distance from the fault results in rocks with young ages exhumed at greater distances from the fault. For example, a 15 km hinge position results in 4–9 Ma ages within 10 km of the fault (Figure 7a). Between 10 and 17 km from the fault samples from the partial annealing zone are exhumed and at distances greater than ~17 km only intrusion ages are present. In contrast, when the hinge is located 40 km from the fault, 4–10 Ma sample ages are present within 30 km of the fault. Ages <10 Ma are present at greater distances from the fault for the 40 km hinge position because the vertical velocity component is larger at any given location in the footwall for a 40 km hinge position than for a 15 km hinge (X_{Hinge}, equation (4)).

[37] The models predict that ages between 10 and 30 km from the fault are sensitive to the position of the hinge. The footwall hinge position could be constrained from samples collected at this distance. Unfortunately, AFT ages collected from the Wasatch Mountains at >18 km from the fault (open circles, Figure 7a) have ages associated with an earlier cooling event in the middle to eastern part of the range

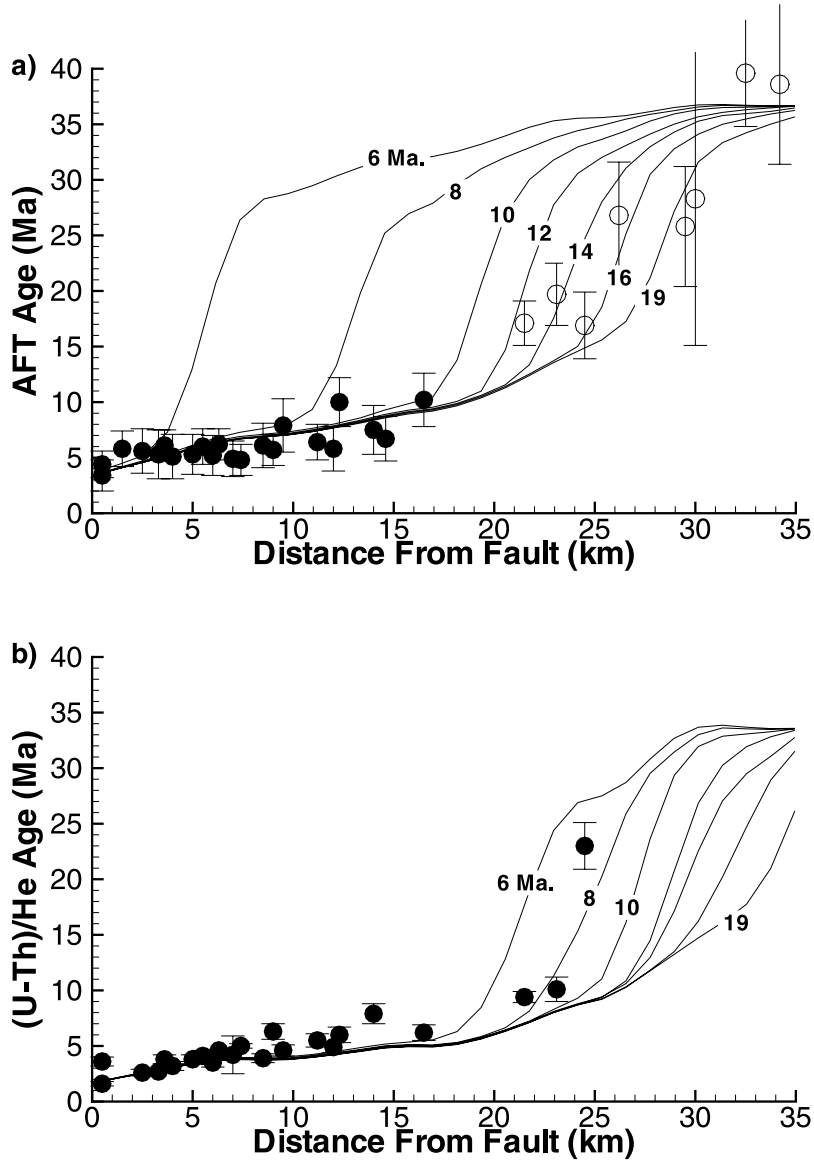

Figure 8. Effect of faulting onset age on predicted thermochronometer ages. Fixed parameters include a 45° dipping fault; a footwall exhumation rate at the fault of 0.8 mm yr^{-1} (equation (3)); and a 25 km footwall hinge position. Solid lines represent predicted (a) AFT and (b) (U-Th)/He ages for onset ages of 6–19 Ma. All samples were assumed to have initial intrusion ages of 35.5 Ma Open circles in Figure 8a represent samples that cooled during an earlier event (see text).

[*Armstrong et al.*, 2003] and therefore provide only a maximum bound on the hinge distance which we infer to be ~25 km from the fault. However, (U-Th)/He ages at distances between ~16.5 and 23.5 km from the fault suggest a footwall hinge location of ~20–25 km from the fault (Figure 7b). This result depends on the simulated exhumation rate of the footwall at the fault (V_{zmax}) and thus is non unique, a point discussed below.

5.4. Effect of Duration of Fault Motion on Ages

[38] Thermochronometer ages also constrain the duration of extension and faulting. The temporal and spatial evolution of exhumed sample ages for samples from a 35 Ma pluton and faulting duration of 6–19 Myr are shown in Figure 8. Other parameters are fixed at 45° for the fault dip, a footwall hinge position of 25 km from the fault, and V_{zmax} of 0.8 mm yr^{-1}. Increasing the duration of faulting results in young ages at greater distances from the fault. For example, if the duration of faulting is 6 Myr, the region of young ages is confined to within ~4 km of fault (Figure 8a). In contrast, if the duration of faulting is 12 Myr, the zone of young ages extends 16 km further into the footwall to a distance of ~20 km from the fault. Samples with young ages are present at progressively greater distances from the fault as the exhumation duration increases because rocks at greater distances are eventually exhumed from below the partial retention zone (PRZ) and will not record their parent (intrusion) age.

[39] Samples with young (U-Th)/He ages also occur at progressively greater distances from the fault with increased duration of faulting (Figure 8b). However, the spatial pattern of ages is different from the AFT age pattern. For example, if the duration of faulting is 6 Myr, rocks with

young ages (3–5 Ma) are exposed to distances of 18 km from the fault. If the duration of faulting is increased to 14 Myr, rocks with young ages are exposed to 26 km from the fault (Figure 8b). The 16 km distance over which rocks with young AFT ages are exposed for faulting durations between 6 and 19 Myr is not present in exhumed (U-Th)/He ages because the helium closure temperature is closer to the surface than for AFT data and the total time between closure and exposure is less.

[40] Comparison between predicted and observed AFT ages in Figure 8a suggests a faulting duration for the Wasatch fault between 10 and 14 Myr. Samples located at >20 km are interpreted to have cooled in an earlier event and therefore provide only a maximum estimate of the cooling duration. The (U-Th)/He data (Figure 8b) suggest an onset of faulting time of 8 Ma, but the lack of samples at >23 km means that this is also only a minimum estimate. The onset time of faulting is discussed in more detail later.

6. Discussion

6.1. Kinematic Model for the Central Wasatch Mountains

[41] The previous sections demonstrate how thermochronometer ages depend on the patterns and rates of footwall uplift as parameterized in the model by fault dip, footwall hinge position, maximum exhumation rate ($V_{z\max}$), and the duration of faulting. The possibility exists that multiple combinations of these parameters can predict the observed ages equally well. Therefore combinations of parameters were investigated over a range of hinge positions from 15 to 40 km, $V_{z\max}$ between 0.2 and 2.0 mm yr$-^{1}$, and fault dip angles of 45° and 60°. We assume an onset time of fault motion consistent with 10 km of vertical exhumation at the fault. The 10 km magnitude of exhumation is consistent with the fluid inclusion results of *Parry and Bruhn* [1987]. Predicted and measured ages were compared using the square root of a reduced chi-square measure of fit

$$\chi^2 = \sqrt{\frac{\sum_{i=1}^{N}\left(\frac{\mathrm{Age}_{p_i} - \mathrm{Age}_{o_i}}{U_i}\right)^2}{N - M}}, \qquad (10)$$

where Age_{p_i} and Age_{o_i} are the predicted and observed AFT or (U-Th)/He ages for the ith point, respectively, U_i is the one standard deviation uncertainty in the ith age; N is the number of samples; and M is the number of model parameters (i.e., 4). Equation (10) provides an unbiased estimator of the root mean square error and a quantified measure of fit. Independent χ^2 values were calculated for AFT and (U-Th)/He ages.

[42] The χ^2 values are shown over the region of parameter space where they vary the most. We plot the values for variations in the footwall hinge position and maximum exhumation rate for each fault dip angle (Figure 9). The χ^2 measures are shown individually for the AFT and (U-Th)/He thermochronometer systems in addition to the combined χ^2 which is the sum of the individual χ^2 measures.

[43] For a 60° dipping fault, the AFT χ^2 = 2 contour spans hinge positions between 25 km and 40 km and footwall exhumation rates at the fault ($V_{z\max}$) between ~0.7 and 1.1 mm yr^{-1}. At the χ^2 = 4 level the (U-Th)/He data (Figure 9b) suggest a $V_{z\max}$ between 0.6 and 0.8 mm yr^{-1} for hinge positions between 25 and 40 km. Similar kinematic parameters are suggested for a 45° fault. Comparison of predicted and observed AFT data suggests hinge positions of between 20 km and 40 km distance from the fault and footwall exhumation rates at the fault ($V_{z\max}$) of ~0.8–1.1 mm yr^{-1} at the χ^2 = 2 level of fit (Figure 9d). The (U-Th)/He ages indicate a $V_{z\max}$ of ~0.6–0.9 mm yr^{-1} for hinge positions between 20 and 40 km (Figure 9e).

[44] The combined AFT and (U-Th)/He chi-square values are shown in Figures 9c and 9f for the 60° and 45° dipping faults, respectively. The best fit model is defined by the lowest combined χ^2 value assuming the model accurately simulates the relevant thermotectonic processes around the Wasatch fault. For a 60° dipping fault the minimum χ^2 value is 4.9 (black box, Figure 9c) and occurs with a 25 km hinge and a $V_{z\max}$ of 0.8 mm yr$-^{1}$. For a 45° dipping fault the combined χ^2 is 4.7 (black box, Figure 10f) and occurs with a hinge at 20 km and with a $V_{z\max}$ of 0.8 mm yr^{-1}. We consider the difference between the 45° and 60° dip combined χ^2 values of 0.2 to be insignificant because of uncertainties in model parameters and assumptions (steady state topography and 2-D thermal field assumptions). We therefore conclude the thermochronometer data are consistent with either fault dip angle. However, a shallow dip angle of ~45° for the Wasatch fault has been inferred from seismic studies [*Smith and Bruhn*, 1984], structural studies [*Bruhn et al.*, 1992], and comparison with average fault dip angles of other normal faults in the Basin and Range [*Jackson and White*, 1989].

[45] One interpretation of the chi-square analysis (Figure 9) is that a decrease in the exhumation rate occurred between closure of the AFT and (U-Th)/He data. For example, comparing Figure 10d and Figure 9e the AFT data suggest a $V_{z\max}$ of 0.9–1.1 mm yr^{-1}, whereas the (U-Th)/He data support a $V_{z\max}$ of 0.7–0.9 mm yr^{-1}. Therefore the exhumation rate could have decreased by several tenths of a millimeter per year sometime since the samples cooled through the AFT PAZ.

[46] We investigated a decrease in the footwall exhumation rate with six additional model simulations. Using a 45° fault and footwall hinge positions of 20 and 25 km, simulations were conducted with a step decrease in $V_{z\max}$ from 1.0 to 0.8 mm yr^{-1} (20 and 25 km hinge positions) and 0.8 to 0.6 mm yr^{-1} (25 km hinge position only). We considered onset times of 6 and 4 Ma for the step decrease in exhumation rate. Chi-square measure of fit was calculated from equation (10) with M = 6 instead of 4 since time and magnitude of the step decrease in exhumation rate are additional parameters. The lowest χ^2values for a step decrease in $V_{z\max}$ are 4.4 and 4.5 and occur with a hinge position of 20 km and a step change in $V_{z\max}$ from 1.0 to 0.8 mm yr^{-1} at 5 Ma, respectively. The maximum exhumation rate of 0.8 mm yr^{-1} from 5 Ma to present is consistent with uplift rates determined from previous studies of offset Quaternary strata exposed fault trenches, assuming that footwall exhumation rates are roughly equivalent to one-half the net tectonic vertical displacement measured in fault-trenches (Table 1).

[47] The previous χ^2 values for simulations with a decrease in the footwall exhumation rates suggest that the

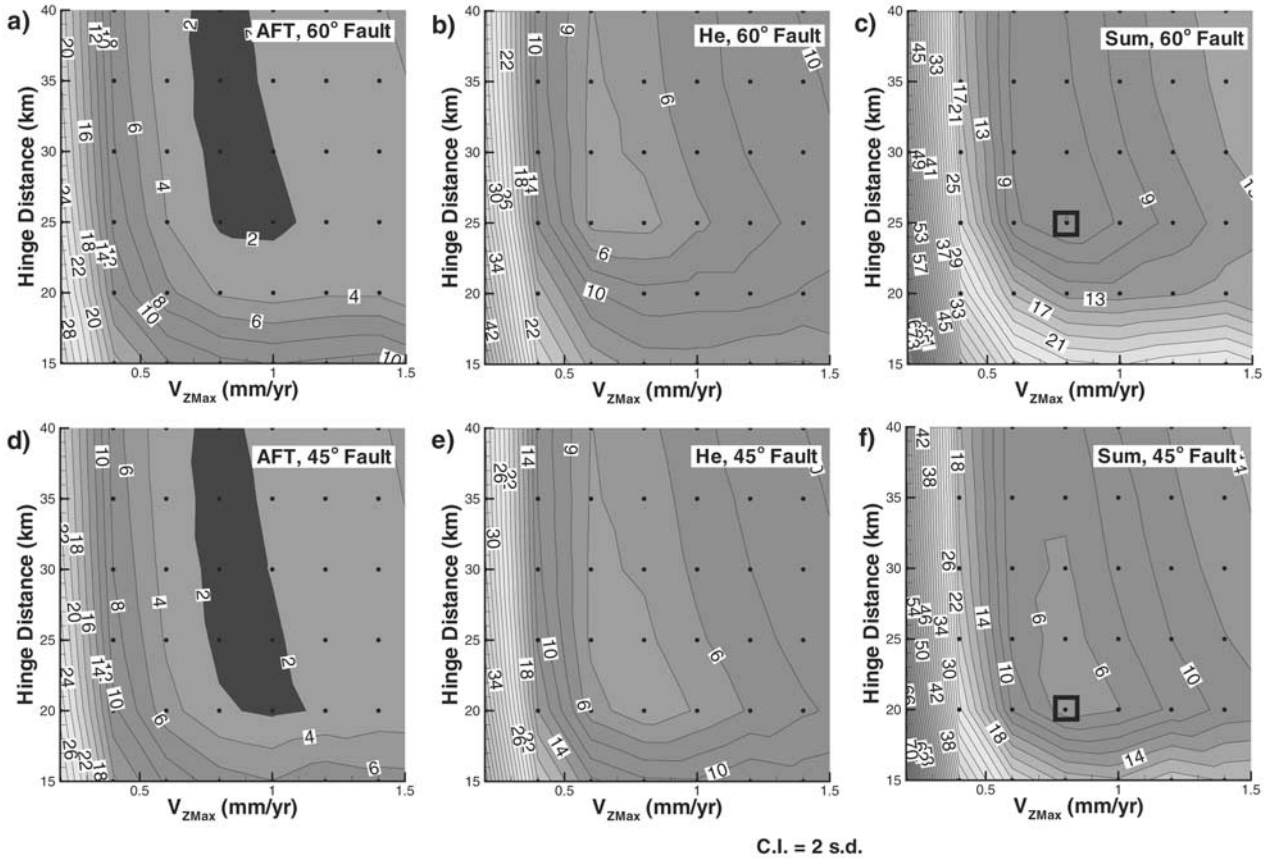

Figure 9. Chi-square measure of fit between predicted and observed thermochronometer ages for the model solution space. (a) AFT, (b) (U-Th)/He, (c) summed AFT and (U-Th)/He misfit for a model with a 60° dipping fault. (d) AFT, (e) (U-Th)/He, (f) summed AFT and (U-Th)/He misfit for a model with a 45° dipping fault. Black boxes in Figures 9c and 9f represent the best fit models.

AFT sample ages were exhumed at an average rate (E_0) of $\sim$1.0 mm yr^{-1} for the last (t_0) $\sim$10 Myr and the (U-Th)/He ages were exhumed at an average rate (E_1) of $\sim$0.8 mm yr^{-1} for the last (t_1) $\sim$5 Ma. Therefore the exhumation rate for the time period between 10 and 5 Ma must have been higher than 1.0 mm yr^{-1}. The exhumation rate (E_2) for the time period between 10 and 5 Ma is given by

$$E_2 = [(E_0 t_0) - (E_1 t_1)](t_0 - t_1)^{-1}. \quad (11)$$

Applying the previous values for E_0, E_1, t_0, and t_1 in equation (11) suggests an exhumation rate of 1.2 mm yr^{-1} between $\sim$10 and 5 Ma. Therefore the thermochronometer data suggest the exhumation rate has decreased by a factor of 1.5 (from 1.2 to 0.8 mm yr^{-1}) at $\sim$5 Ma.

[49] The model-derived maximum exhumation rate of 0.8 mm yr^{-1} at the fault suggests and average exhumation rate of 0.7 mm yr^{-1} between 0 and 5 km distance from the fault (assuming tilt on a hinge located 20 km from the fault). This exhumation rate is almost a factor of 2 less than that implied by the local north-south elevation-age change from ridge top to canyon bottom in Figure 5b of *Armstrong et al.* [2003]. This discrepency may indicate a ridge to canyon topographic effect on subsurface isotherms and/or that the landscape is not in steady state over the timescale of $\sim$4 Myr (the mean sample age) [e.g., see *Braun*, 2002].

6.2. Onset of Faulting and Maximum Temperatures of Exposed Rocks

[50] We infer that the Wasatch fault has been active for 10–12 Myr with a maximum exhumation rate between 0.8 and 1.0 mm yr^{-1} based on the distribution of ages in the footwall (section 5.4 and 6.1). This fault onset time is also constrained by considering the maximum temperature experienced by exhumed rocks. We now use the distribution of ZFT, AFT, (U-Th)/He ages across the footwall to delineate the exhumation duration of the Wasatch fault footwall. Despite uncertainties in the kinetics of ZFT annealing the temperature range encompassing the ZFT PAZ is inferred to be between $\sim$230–330°C [*Yamada et al.*, 1995]. As discussed below, this temperature range of the ZFT PAZ allows us to use the distribution of ZFT ages from the Wasatch mountains to interpret the duration of exhumation.

[51] Figure 10 shows predicted maximum temperatures of rocks exposed at the surface as a function of distance from the fault with different ages of initiation of fault motion. As with previous models, footwall tilt implies that rocks exhumed adjacent to the fault experienced higher maximum temperatures than rocks exhumed at greater distances from the fault (Figure 10a). For an onset time of faulting less than

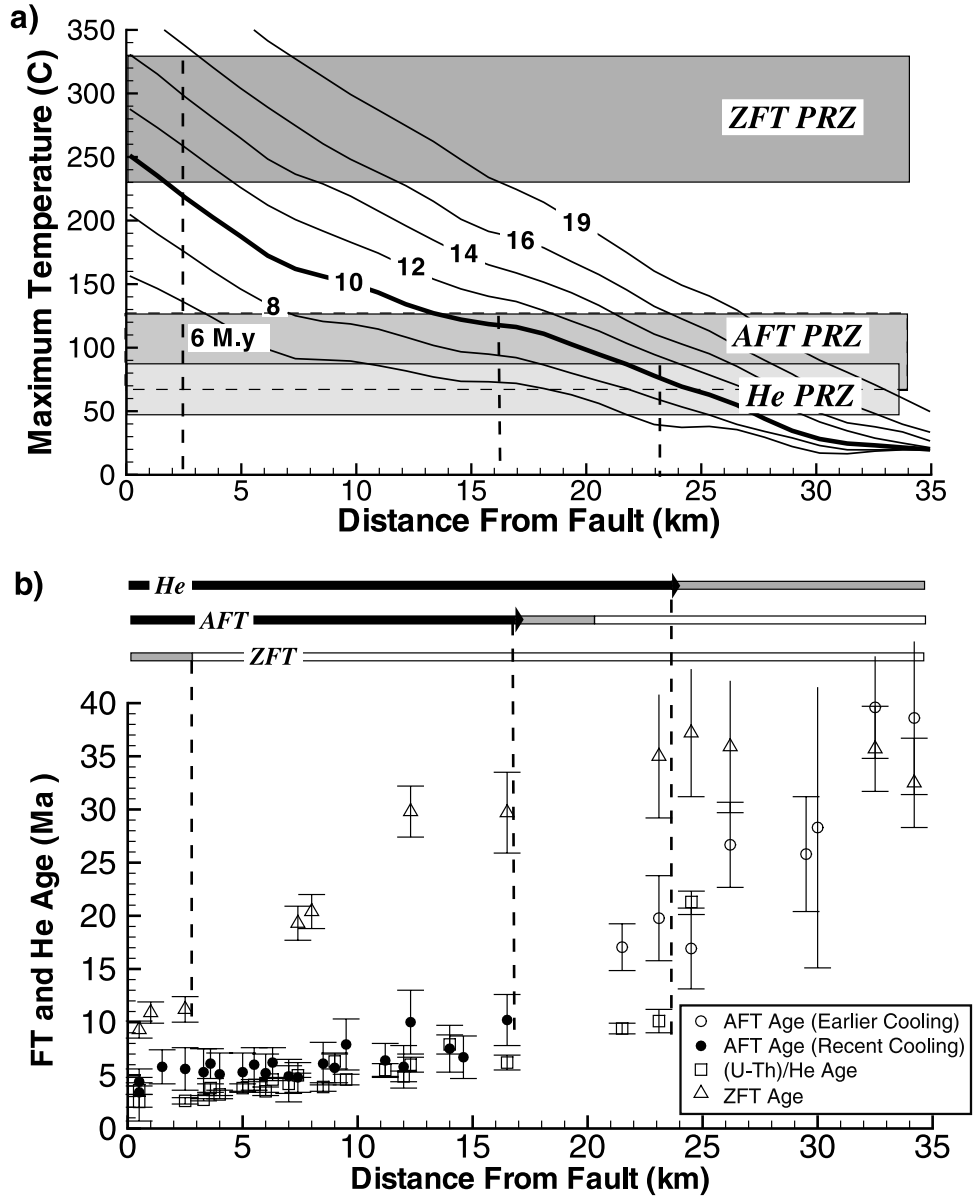

Figure 10. Predicted maximum temperature experienced by a surface rock as a function of distance from the fault and time since initiation of fault motion. Model includes fixed parameters of a 45° dipping fault, 25 km footwall hinge, and footwall exhumation rate at the fault of 0.8 mm yr^{-1} (V_{zmax}, equation (3)). (a) Maximum exhumed temperatures (solid lines) across the footwall for faulting onset times between 6 and 19 Ma. Horizontal shaded boxes represent the approximate temperature range of the PRZ. (b) Thermochronometer ages versus distance from fault. Horizontal black, gray, and white bars represent the observed lateral extent of samples exhumed from depths below, within, and above the PRZ, respectively.

~8 Myr a rock exhumed adjacent to the fault would originate from above the ZFT PAZ and would thus have a ZFT age equivalent to the intrusion age (35 Ma). However, if faulting persisted for longer than 8 Myr, a sample from the footwall adjacent to the fault would originate from within the ZFT PAZ and would therefore have a ZFT age younger than the intrusion age. This pattern holds for the other thermochronometer systems as well.

[52] Wasatch Mountain samples that we interpret as having been exhumed from below, within, and above the PAZ or PRZ are shown in Figure 10b. The horizontal bars indicate distance from the fault that we predict ages to reflect exhumation from different depths. For onset of faulting at 10 Ma, ZFT ages of rocks exposed at <3 km from the fault experienced maximum temperatures between 220 and 250°C. ZFT ages of rocks exposed between 3 and 9 km distance experienced maximum temperatures between 150 and 220°C. ZFT ages of rocks exposed at >9 km distance experienced maximum temperatures <150°C. For the same onset of faulting time, AFT ages in rocks exposed at <17 km distance experienced maximum temperatures >110°C. No AFT ages associated with this episode of

Table A1. Heat Production Measurements

Formation	Lithology	Sample	Density, g/cm^{-3}	Potassium, wt%	Uranium, ppm	Thorium, ppm	Heat Production, μWm^{-3}
Farmington Canyon	metamorphic	A	2.7	3.0	2.7	23.9	2.8
		B	3.0	0.8	1.1	2.5	0.6
		C	2.7	3.4	2.3	25.9	2.7
		D	2.9	1.2	1.0	5.8	0.8
		E	2.7	1.0	1.7	14.1	1.5
Little Willow	metamorphic	A	2.6	0.2	0.2	0.6	0.1
		B	2.7	1.0	1.2	6.9	0.9
		C	2.8	3.3	1.8	7.5	1.3
		D	3.0	0.5	0.3	2.0	0.3
		E	2.9	0.6	0.4	1.6	0.3
Little Cottonwood	monzonitet	A	2.7	2.9	3.9	10.8	2.0
		B	2.6	3.5	2.7	10.8	1.7
Alta Stoc	monzonite	A	2.7	2.5	4.0	12.0	2.1
		B	2.7	2.4	3.3	10.4	1.8
Ankareh	shale	A	2.7	4.1	1.4	8.1	1.3
Big Cottonwood	argillite	A	2.8	1.9	4.2	15.3	2.4
		B	2.7	2.0	2.7	11.1	1.7
Ophir	shale	A	2.8	6.0	3.5	16.5	2.8
Mancos	shale	A	2.4	1.6	2.9	8.1	1.3
Kelvin	sandstone	A	2.4	0.3	0.7	1.6	0.3

cooling are observed at distances >17 km. (U-Th)/He ages of rocks present at distances <23 km from the fault experienced temperatures >70°C. No (U-Th)/He ages are available at distances >23 km from the fault where predicted maximum temperatures are <80°C.

[53] *Armstrong et al.* [2003] interpret the ZFT ages within 3 km of the fault as originating in, or below, the ZFT PAZ. If the ZFT ages within 3 km of the fault originated from within the ZFT PAZ then these sample had maximum temperatures somewhere between 230 and 330°C. Rocks with ZFT ages with this range of maximum temperatures would only be exposed if the onset of faulting was between 9 and 14 Ma. The AFT samples exposed within 17 km of the fault have ages <11 Ma and are interpreted as exhumed from depths below the AFT PAZ. The 10 Ma AFT age of the sample at 17 km from the fault implies a minimum faulting onset age of 10 Ma On the basis of the inferred maximum temperatures of the ZFT and AFT data we interpret a faulting onset age of 12 ± 2 Ma.

[54] This 12 Ma onset age of faulting is sensitive to the assumption of steady state topography and the use of the present-day topography of the Wasatch Mountains as the initial condition in the thermokinematic model. A more realistic assumption would be that the present-day topography of the Wasatch Mountains evolved over the first couple million years of faulting [*Densmore et al.*, 1998; *Allen and Densmore*, 2000], in which case exhumation and erosion rates would be less over this time period. If this were the case and the topography developed over the first several million years than our assumed initial condition of steady state topography could result in the predicted onset time of faulting to be under estimated by ~1–2.5 Myr.

[55] Nevertheless, assuming an onset age of 12 Ma and a maximum exhumation rate (V_{zmax}) of 0.8 mm yr^{-1}, we infer an exhumation magnitude of 9.6 km ~± 1.6 km) at the fault. This exhumation magnitude and predicted maximum temperatures of 250–330°C for samples exhumed adjacent to the fault (Figure 10a) are consistent with maximum temperatures and pressures measured in fluid inclusion samples from the Wasatch fault [*Parry et al.*, 1988].

7. Conclusions

[56] Many exhumation studies in normal fault bounded ranges commonly use the slope of a best fit line in a plot of thermochronometer sample age versus elevation to delineate the apparent exhumation rate. Although this approach is useful for determining an approximate exhumation rate it is seldom able to quantify other important kinematic parameters such as spatial and temporal variations in the true exhumation rate, fault dip angle, footwall tilt, or exhumation duration. The previous kinematic parameters are of interest

Table A2. Thermal Conductivity Measurements

Formation	Lithology	*N*	Whole Rock Conductivity, W m^{-1} K^{-1}	1 SD, W m^{-1} K^{-1}	Porosity, %	Matrix Conductivity, W m^{-1} K^{-1}	1 SD, W m^{-1} K^{-1}
Little Cottonwood	monzonite	4	2.8	0.14	1.3	2.8	0.14
Ophir Shale	shale	4	3.1	1.28	0.6	3.1	1.30
Twin Creek	limestone	5	2.6	0.13	0.8	2.7	0.17
Farmington Canyon	metamorphic	6	3.2	0.64	0.9	3.2	0.63
Gaurdison	limestone	4	3.5	0.38	0.4	3.6	0.39
Nugget	sandstone	3	6.2	0.26	1.9	6.5	0.51
Kelvin	sandstone	5	4.7	0.38	14.0	6.5	0.47
Big Cottonwood	quartzite	3	6.7	0.81	1.2	6.9	0.84
Ankareh	sandstone	3	4.6	0.58	3.9	5.0	0.33
Little Willow	metamorphic	5	3.7	2.30	0.9	3.8	2.39

when trying to understand the structural and geodynamic evolution of rift environments around the world. The approach presented in this study differs from that of many other thermochronometer studies in that we integrate thermochronometer data and numerical models to quantify the kinematic evolution of a normal fault bounded range.

[57] We coupled 2-D thermal, kinematic, and thermochronometer kinetic models to describe the distribution of exhumed ZFT, AFT, and (U-Th)/He sample ages in the Cottonwood Intrusive Belt in the central Wasatch Mountains. The modeling approach employed in this study is applicable to studies of normal fault bounded ranges in other rift environments. Our consideration of 2-D particle trajectories and thermal histories of exhumed thermochronometer samples lead to the following conclusions:

1. AFT and (U-Th)/He ages can be explained by models with a constant rate of exhumation or by models with a decrease in the exhumation rate. The best fit, constant-exhumation model has a rate of 0.8 mm yr^{-1} at the fault and an age of onset of 12 Ma. A slightly better fit is found for a model with the maximum exhumation rate of 1.2 mm yr^{-1} for the time period between ~10 and 5 Ma. For the last 5 Myr, there appears to be a factor of 1.5 decrease in the maximum exhumation rate to 0.8 mm yr^{-1}.

2. The distribution of ZFT, AFT, and (U-Th)/He ages of rocks exposed across the footwall suggests a faulting onset time of 12 ± 2 Myr This onset time and a constant maximum exhumation rate 0.8 mm $yr-^{1}$ predict 9 ± 1.6 km of exhumation at the fault. This magnitude of exhumation is consistent with previous studies of the maximum pressures and temperatures inferred from fluid inclusions in rocks near the Wasatch fault.

3. Tilt of the Wasatch Mountains occurs around a structural hinge such that exhumation rates are highest adjacent to the fault and decrease toward the hinge [e.g., *Armstrong et al.*, 2003]. Model results suggest the Wasatch Mountains to have a footwall hinge located at a minimum of 20–25 km from the footwall.

Appendix A: Thermophysical Property Measurements

[58] Radiogenic heat production was measured in 20 samples from nine formations in the Wasatch Mountains (Table A1). Heat production measurements were made by D. Pribnow at the thermophysical properties laboratory, Hannover, Germany, using a Canberra multichannel analyzer, series 35, model 3201, with a 3″ × 3″ NaI detector. Heat production was derived from the content of U, Th, and K. The quantities of these elements were derived from the gamma ray spectrum measured on 2 kg samples crushed to <1 cm diameter.

[59] Thermal conductivity measurements were conducted on 42 samples from 10 formations in the central Wasatch Mountains. These samples augmented 800 thermal conductivity measurements previously made on lithologies located in northcentral Utah and present near the central Wasatch Mountains [*Deming*, 1988; *Bodell and Chapman*, 1982; *Moran*, 1991; *Powell*, 1997]. Conductivity measurements (Table A2)] were made at room temperature on samples >10 cm in diameter using a TK-04 line source at the University of Utah. Two orthogonal measurements were made on each sample to determine if samples were anisotropic. Anisotropy was not detected in any of the samples.

[60] **Acknowledgments.** This research was funded by a University of Utah Graduate Research Fellowship (to Ehlers) and NSF grant EAR-9805073 (To Armstrong and Chapman). Daniel Pribnow (Shell International) is acknowledged for measurement of radiogenic heat production and specific heat. This manuscript benefited from reviews by Geoff Batt, associate editor Jean Braun, and an anonymous reviewer.

References

Allen, P. A., and A. L. Densmore, Sediment flux from an uplifting fault block, *Basin Res.*, *12*, 367–380, 2000.

Arabasz, W. J., J. C. Pechmann, and E. D. Brown, Observational seismology and the evaluation of earthquake hazards and risk in the Wasatch Front area, Utah, in *Assessment of Regional Earthquake Hazards and Risk Along the Wasatch Front, Utah*, edited by P. L. Gori and W. W. Hays, *U.S. Geol. Surv. Prof. Pap., 1500-A-J*, D1–D36, 1992.

Armstrong, P. A., T. A. Ehlers, D. S. Chapman, K. A. Farley, and P. J. J. Kamp, Exhumation of the central Wasatch Mountains, Utah: 1. Patterns and timing deduced from low-temperature thermochronology data, *J. Geophys. Res.*, *108*, doi:10.1029/2001JB001708, in press, 2003.

Batt, G. E., and M. T. Brandon, Lateral thinking: 2-D interpretations of thermochronology in convergent orogenic settings, *Tectonophysics*, *349*, 185–201, 2001.

Batt, G. E., M. T. Brandon, K. A. Farley, and M. Roden-Tice, Tectonic synthesis of the Olympic Mountains segment of the Cascadia wedge, using two-dimensional thermal and kinematic modeling of thermochronological ages, *J. Geophys. Res.*, *106*, 26,731–26,746, 2001.

Bertotti, G., and M. ter Voorde, Thermal effects of normal faulting during rifted basin formation, 2, The Lugano-Val Grande normal fault and the role of pre-existing thermal anomalies, *Tectonophysics*, *240*, 145–157, 1994.

Bodell, J. M., Heat flow in the north-central Colorado Plateau, M.S. thesis, 134 pp., Dep. of Geol. and Geophys., Univ. of Utah, Salt Lake City, 1981.

Bodell, J. M., and D. S. Chapman, Heat flow in the north-central Colorado Plateau, *J. Geophys. Res.*, *87*, 2869–2884, 1982.

Braun, J., Quantifying the effect of recent relief changes on age-elevation relations, *Earth Planet. Sci. Lett.*, *200*, 331–343, 2002.

Bruhn, R. L., P. R. Gibler, W. Houghton, and W. T. Parry, Structure of the Salt Lake segment, Wasatch normal fault zone: Implications for rupture propagation during normal faulting, in *Assessment of Regional Earthquake Hazards and Risk Along the Wasatch Front, Utah*, edited by P. L. Gori and W. W. Hays, *U.S. Geol. Surv. Prof. Pap., 1500-A-J*, H1–H25, 1992.

Buntebarth, G., Thermal properties of KTB Oberpfalz—VB core samples at elevated temperature and pressure, *Sci. Drill.*, *2*, 73–80, 1991.

Carlson, W. D., Mechanisms and kinetics of apatite fission-track annealing, *Am. Mineral.*, *75*, 1120–1139, 1990.

Carlson, W. D., R. A. Donelick, and R. A. Ketcham, Variability of apatite fission-track annealing kinetics, I, Experimental results, *Am. Mineral.*, *84*, 1213–1223, 1999.

Carslaw, H. S., and J. C. Jaeger, *Conduction of Heat in Solids*, Oxford Univ. Press, New York, 1959.

Clauser, C., and E. Huenges, Thermal conductivity of rocks and minerals, in *Rock Physics and Phase Relations: A Handbook of Physical Constants*, *AGU Ref. Shelf*, vol. 3, edited by T. J. Ahrens, pp. 105–126, AGU, Washington, D. C., 1995.

Constenius, K. N., Extensional tectonics of the Cordilleran foreland fold and thrust belt and the Jurassic-Cretaceous Great Valley forearc basin, Ph.D. thesis, Univ. of Ariz., Tuscon, 1998.

Crittenden, M. D., Jr., General geology of Salt Lake County, Sec. 1., bulletin, Utah Geol. and Mineral. Surv., Salt Lake City, Utah, 1964.

Crone, A., and S. T. Harding, Near-surface faulting associated with Holocene fault scarps, Wasatch fault zone, Utah; a preliminary report, in *Proceedings of Conference XXVI; A Workshop on Evaluation of Regional and Urban Earthquake Hazards and Risk in Utah*, edited by W. W. Hay and P. L. Gori, *U.S. Geol. Surv. Open File Rep., 87–585*, 23–56, 1987.

Crowley, K. D., M. Cameron, and R. L. Schaefer, Experimental studies of annealing of etched fission tracks in flourapatite, *Geochim. Cosmochim. Acta*, *55*, 1449–1465, 1991.

Davis, W. M., The mountain ranges of the Great Basin, *Harvard Univ. Mus. Comparative Zoology Bull.*, *42*, 127–175, 1903.

Deming, D., Geothermics of the thrust belt in north-central Utah, Ph.D. thesis, 197 pp., Univ. of Utah, Salt Lake, 1988.

Densmore, A. L., M. A. Ellis, and R. S. Anderson, Landsliding and the evolution of normal-fault bounded mountains, *J. Geophys. Res.*, *103*, 15,203–15,219, 1998.

Donelick, R. A., R. A. Ketcham, and W. D. Carlson, Variability of apatite fission track annealing kinetics, II, Crystallographic orientation effects, *Am. Mineral.*, *84*, 1224–1234, 1999.

Eardley, A. J., Strong relief before block faulting in the vicinity of the Wasatch Mountains, Utah, *J. Geol.*, *41*, 243–267, 1933.
Eardley, A. J., Structure of the Wasatch-Great Basin region, *Geol. Soc. Am. Bull.*, *50*, 1277–1310, 1939.
Ehlers, T. A., and M. A. Chan, Tidal sedimentology and estuarine deposition of the proterozoic Big Cotton Wood Formation, Utah, *J. Sediment. Res.*, *69*, 1169–1180, 1999.
Ehlers, T. A., and D. S. Chapman, Normal fault thermal regimes: Conductive and hydrothermal heat transfer surrounding the Wasatch fault, Utah, *Tectonophysics*, *312*, 217–234, 1999.
Ehlers, T. A., P. A. Armstrong, and D. S. Chapman, Normal fault thermal regimes and interpretation low- temperature thermochronometer data, *Phys. Earth Planet. Inter.*, *126*, 179–194, 2001.
Evans, S. H., W. T. Parry, and R. L. Bruhn, Thermal, mechanical and chemical history of Wasatch fault cataclasite and phyllonite, Traverse Mountains area, Salt Lake City, Utah: Age and uplift rates from K/Ar and fission track measurements, *U.S. Geol. Surv. Open File Rep.*, *86–31*, 410–415, 1985.
Farley, K. A., Helium diffusion from apatite: General behavior as illustrated by Durango flourapatite, *J. Geophys. Res.*, *105*, 2903–2914, 2000.
Farley, K. A., R. A. Wolf, and L. T. Silver, The effects of long alpha-stopping distances on (U-Th)/He ages, *Geochim. Cosmochim. Acta*, *60*, 4223–4229, 1996.
Gilbert, G. K., Studies of basin-range structure, *U.S. Geol. Surv. Prof. Pap.*, *153*, 89 pp., 1928.
Gleadow, A. J. W., and R. W. Brown, Fission-track thermochronology and the long-term denudational response to tectonics, in *Geomorphology and Global Tectonics*, edited by M. A. Summerfield, pp. 57–73, John Wiley, New York, 2000.
Grasemann, B., and N. S. Mancktelow, Two dimensional thermal modelling of normal faulting: The Simplon Fault Zone, central Alps, Switzerland, *Tectonophysics*, *225*, 155–165, 1993.
Green, P. F., I. R. Duddy, A. J. W. Gleadow, P. R. Tingate, and G. M. Laslett, Fisson track annealing in apatite track length measurements and the form of the Arrhenius plot, *Nucl. Tracks*, *10*, 323–328, 1985.
Green, P. F., I. R. Duddly, A. J. W. Gleadow, P. R. Tingate, and G. M. Laslett, Thermal annealing of fission tracks in apatite, 1, A qualitative description, *Chem. Geol.*, *59*, 237–253, 1986.
Hecker, S., Quaternary tectonics of Utah with emphasis on earthquake hazard characterization, *Utah Geol. Surv. Bull.*, *127*, 157 pp., 1993.
Hintze, L. F., Wasatch fault zone east of Provo, Utah, in Environmental geology of the Wasatch front, edited by L. S. Hipert, Utah Geol. Assoc. Publ., 1, F1–F10, 1971.
Jackson, J. A., and N. J. White, Normal faulting in the upper continental crust; observations from regions of active extension, *J. Struct. Geol.*, *11*, 15–36, 1989.
John, D. A., Geologic setting, depths of emplacement, and regional distribution of fluid inclusions in intrusions of the central Wasatch Mountains, *Utah, Econ. Geol.*, *84*, 386–409, 1989.
Keaton, J. R., D. R. Currey, and S. S. Olig, Paleoseismicity and earthquake hazards evaluation of the West Valley fault zone, Salt Lake City urban area, Utah, contract report 93-8, 55 pp., Utah Geol. Surv., Salt Lake City, 1993.
Ketcham, R. A., D. A. Donelick, and W. D. Carlson, Variability of apatite fission-track annealing kinetics, III, Extrapolation to geological time scales, *Am. Mineral.*, *84*, 1235–1255, 1999.
King, C., *Systematic Geology: Report of the Geological Exploration of the 40th Parallel*, vol. 1, 803 pp., U.S. Govt. Print. Off., Washington, D.C., 1878.
Kowallis, B. J., J. Ferguson, and G. J. Jorgensen, Uplift along the Salt Lake segment of the Wasatch fault from apatite and zircon fission track dating in the Little Cottonwood Stock, *Nucl. Tracks Radiat. Meas.*, *17*, 325–329, 1990.
Lachenbruch, A., and J. H. Sass, Heat flow in the United States and the thermal regime of the crust, in *The Earth's Crust: Its Nature and Physical Properties*, *Geophys. Monogr. Ser.*, vol. 20, edited by J. G. Heacock et al., pp. 626–675, AGU, Washington D.C., 1977.
Laslett, G. M., P. F. Green, I. R. Duddy, and A. J. W. Gleadow, Thermal annealing of fission tracks in apatite, 2, A quantitative analysis, *Chem. Geol.*, *65*, 1–13, 1987.
Machette, M. N., S. F. Personius, and A. R. Nelson, Paleoseismology of the Wasatch fault zone: A summary of recent investigations, interpretations, and conclusions, in *Assessment of Regional Earthquake Hazards and Risk Along the Wasatch Front, Utah*, edited by P. L. Gori and W. W. Hays, *U.S. Geol. Surv. Prof. Pap. 1500 A-J*, A1–A71, 1991.
Mancktelow, N. S., and B. Grasemann, Time-dependent effects of heat advection and topography on cooling histories during erosion, *Tectonophysics*, *270*, 167–195, 1997.
Marsell, R. E., Geology of the Jordan Narrows region, Traverse Mountains, UT, M.S. thesis, 88 pp., Univ. of Utah, Salt Lake City, 1932.
McCalpin, J. P., and S. P. Nishenko, Holocene paleoseismicity, temporal clustering, and probabilities of future large (M > 7) earthquakes on the Wasatch fault zone, Utah, *J. Geophys. Res.*, *101*, 6233–6253, 1996.
Moran, K. J., Shallow thermal regime at the Jordanelle dam site, Central Rocky Mountains, Utah, Master's thesis, 141 pp., Univ. of Utah, Salt Lake City, 1991.
Naeser, C. W., Thermal history of sedimentary basins by fission track dating of sub-surface rocks, in *Aspects of Diagenesis*, edited by P. A. Scholle and P. R. Schulger, *Spec. Publ. Soc. Econ Paleont. Mineral.*, *26*, 109–112, 1979.
Naeser, C. W., and H. Faul, Fission track annealing in apatite and sphere, *J. Geophys. Res.*, *74*, 705–710, 1969.
Naeser, N. D., C. W. Naeser, and T. H. McCulloh, The application of fission-track dating to depositional and thermal history of rocks in sedimentary basins, in *Thermal History of Sedimentary Basins - Methods and Case Histories*, edited by N. D. Naeser and T. H. McCulloh, pp. 157–180, Springer- Verlag, New York, 1989.
Ozisik, M. N., *Boundary Value Problems of Heat Conduction*, Dover, Mineola, N. Y., 1989.
Parrish, R. R., Cenozoic thermal evolution and tectonics of the coast mountains of British Columbia 1. Fission track dating apparent uplift rates, and patterns of uplift, *Tectonics*, *2*, 601–631, 1983.
Parry, W. T., and R. L. Bruhn, Fluid inclusion evidence for minimum 11 km vertical offset on the Wasatch fault, Utah, *Geology*, *15*, 67–70, 1987.
Parry, W. T., P. Wilson, and R. L. Bruhn, Pore fluid chemistry and chemical reactions on the Wasatch normal fault, Utah, *Geochim. Cosmochim. Acta*, *52*, 2053–2063, 1988.
Powell, W. G., Thermal state Colorado Plateau-Basin and Range transition, Ph.D. thesis, 232 pp., Univ. of Utah, Salt Lake City, 1997.
Radkins, H., Inversion of bedrock topography in Salt Lake Valley from gravity data, Master of science thesis, 59 pp., Univ. of Utah, Salt Lake City, 1990.
Sass, J. H., A. H. Lachenbruch, and P. Morgan, Thermal regime of the southern Basin and Range province, 1, Heat flow data from Arizona and Mohave desert of California and Nevada, *J. Geophys. Res.*, *99*, 22,093–22,119, 1994.
Schwartz, D. P., and K. J. Coppersmith, Fault behavior and characteristic earthquakes; examples from the Wasatch and San Andreas fault zones, *J.*Geophys. Res., *89*, 5681–5698, 1984.
Smith, R. B., and R. L. Bruhn, Intraplate extensional tectonics of the eastern Basin-Range: Inferences on structural style from seismic reflection data, regional tectonics, and thermal-mechanical models of brittle-ductile deformation, *J. Geophys. Res.*, *89*, 5733–5762, 1984.
Stüwe, K. L., and M. Hintermüller, Topography and isotherms revisited: The influence of laterally migrating drainage divides, *Earth Planet. Sci. Lett.*, *184*, 287–303, 2000.
Stüwe, K., L. White, and R. Brown, The influence of eroding topography on steady-state isotherms. Applications to fission track analysis, *Earth Planet. Sci. Lett.*, *124*, 63–74, 1994.
Swan, F. H., III, D. P. Schwartz, and L. S. Cluff, Recurrence of moderate to large magnitude earthquakes produced by surface faulting on the Wasatch fault zone, Utah, *Bull. Seismol. Soc. Am.*, *70*, 1431–1462, 1980.
ter Voorde, M., and G. Bertotti, Thermal effects of normal faulting during rifted basin formation, 1, A finite difference model, *Tectonophysics*, *240*, 133–144, 1994.
van Wees, J. D., K. deJong, and S. Cloetingh, Two-dimensional P-T-t modelling and the dynamics of extension and inversion in the Beltic Zone (SE Spain), *Tectonophysics*, *203*, 305–324, 1992.
Wagner, G. A., and G. M. Reimer, Fission track tectonics; the tectonic interpretation of fission track apatite ages, *Earth Planet. Sci. Lett.*, *14*, 263–268, 1972.
Willett, S. D., Modelling thermal annealing of fission tracks in apatite, in *Mineralogical Association of America Short Course on Low Temperature Thermochronology: Techniques and Applications*, edited by M. Zentilli, pp. 43–72, Mineral. Assoc. of Am., Washington, D. C., 1992.
Willett, S. D., Inverse modeling of annealing of fission tracks in apatite, 1, A controlled random search method, *Am. J. Sci.*, *297*, 939–969, 1997.
Wolf, R. A., K. A. Farley, and L. T. Silver, Helium diffusion and low-temperature thermochronometry of apatite, *Geochim. Cosmochim. Acta*, *60*, 4231–4240, 1996.
Wolf, R. A., K. A. Farley, and D. M. Kass, Modeling of the temperature sensitivity of the apatite (U-Th)/He thermochronometer, *Chem. Geol.*, *148*, 105–114, 1998.
Yamada, R., T. Tagami, S. Nishimura, and H. Ito, Annealing kinetics of fission tracks in zircon: An experimental study, *Chem. Geol.*, *122*, 249–258, 1995.
Zeitler, P. K., A. L. Herczig, I. McDougall, and M. Honda, U-Th-He dating of apatite: A potential thermochronometer, *Geochim. Cosmochim, Acta*, *51*, 2865–2868, 1987.
Zoback, M. L., Structure and Cenozoic tectonism along the Wasatch fault zone, Utah, in *Tectonics and Stratigraphy of the Eastern Great Basin*,

edited by D. M. Miller, V. R. Todd, and K. A. Howard, *Mem. Geol. Soc. Am.*, *157*, 3–37, 1983.

D. S. Chapman, Department of Geology and Geophysics, University of Utah, 135 S., 1460 E., Salt Lake City, UT 84112, USA. (dchapman@mines.utah.edu)

S. D. Willett, Department of Earth and Space Sciences, University of Washington, Box 351310, Seattle, WA 98195, USA.

P. A. Armstrong, Department of Geological Sciences, California State University, Fullerton, P.O. Box 6850, Fullerton, CA 92834, USA. (parmstrong@fullerton.edu)

T. A. Ehlers, Department of Geological Sciences, University of Michigan, 2534 C.C. Little Building, 425 East University, Ann Arbor, MI 48109-1063, USA. (tehlers@umich.edu)